1975

Experimental study of electron density and confinement time in an electrostatically-plugged cusp device using a microwave interferometer

Robert Louis Hayward

Recommended Citation

EXPERIMENTAL STUDY OF ELECTRON DENSITY AND

CONFINEMENT TIME IN AN ELECTROSTATICALLY-PLUGGED

CUSP DEVICE USING A MICROWAVE INTERFEROMETER

BY

ROBERT LOUIS HAYWARD, 1946-

A THESIS

Presented to the Faculty of the Graduate School of the

UNIVERSITY OF MISSOURI-ROLLA

In Partial Fulfillment of the Requirements for the Degree

MASTER OF SCIENCE IN NUCLEAR ENGINEERING

1975

Approved by

T. J. Dolan (Advisor) _John T. Park_

Robert E. Bolon

ABSTRACT

The average electron density and electron confinement time in an electrostatically plugged magnetic spindle cusp device are studied using a 20 GHz microwave interferometer. The results are compared with the predictions from approximate theoretical equations. With a magnetic induction in the point cusp of 5000 Gauss, a plasma is produced by injecting a 5 mA, 500 eV electron beam into hydrogen gas at 10^{-5} Torr. The measured electron density is 2×10^{10} cm^{-3} and the measured confinement time is 80 μsec, which agree to within a factor of two with values predicted by theory.

ACKNOWLEDGEMENTS

TABLE OF CONTENTS

TABLE OF CONTENTS (cont.)

LIST OF TABLES

LIST OF ILLUSTRATIONS

LIST OF SYMBOLS

$\vec{a}$	Acceleration of individual particles.
a	Ratio of the electron cyclotron frequency to the microwave frequency.
a_p	Radius of point anode gap.
a_r	Half-width of ring anode gap.
$\vec{B}$	Magnetic field component of the electromagnetic wave.
$\vec{B}_1$	Space-and-time perturbed magnetic field.
$\tilde{B}_1$	Amplitude of B_1
$\vec{B}_0$	Externally applied magnetic field.
B_r, B_z	Magnetic induction in the ring and point cusp regions.
b	Ratio of the plasma frequency to the microwave frequency.
c	Speed of light.
c^2	Sum of a^2 and b^2.
d_1	Half-width of electron cloud in the ring anode.
$\vec{E}$	Electric field component of the electromagnetic wave.
$\vec{E}_1$	Space-and-time perturbed electric field.
$\tilde{E}_1$	Amplitude of E_1.
e	Electronic charge in units of esu.
$\vec{F}$	Force on an individual particle.
f	Distribution function.
f_1	The fraction of Φ_A equal to $\Delta\Phi$.
f_2	The number of Larmor radii equal to the radius of the electron cloud in the point anode.
f_3	The fraction of the electron injection energy equal to the electron energy perpendicular to the magnetic field.

LIST OF SYMBOLS (cont.)

$\vec{I}$ Identity matrix.

I_e Electron injection current.

i $(-1)^{1/2}$

$\vec{J}$ Current density.

$\vec{J}_1$ Space-and-time perturbed current density.

$\tilde{J}_1$ Amplitude of $\vec{J}_1$.

$\vec{k}$ Vector wave number of electromagnetic wave.

k_p, k_v Wave number of electromagnetic wave propagating through

                   a plasma and a vacuum.

k_{ord}, k_{ex},   Wave number for the ordinary, extraordinary, and the

$k_{l,r}$ left-right hand circularly polarized electromagnetic waves.

L   Thickness of a plasma.

m   Mass of the particle under consideration.

$\bar{n}$ Average density, average electron density.

n   Particle density.

n_A Electron density in the anode.

n_c Critical electron density as defined by plasma frequency

                   relation.

n_e Electron density.

n_m Neutral atom density.

n_α Density of particles of species α.

$\vec{P}_1$ Anisotropic component of the pressure tensor.

$\vec{P}$ Pressure tensor.

p   Scalar equilibrium pressure.

$\vec{Q}$ Heat flow tensor.

LIST OF SYMBOLS (cont.)

q_α	Electronic charge of species α in units of esu.
R	Ring anode radius.
$\vec{r}$	Space coordinate.
r_L	Average Larmor radius.
r_{Lmax}	Distance between the centerline in the ring anode and the magnetic field line that grazes an anode surface.
r_{Lp}, r_{Lr}	Average Larmor radius in point and ring anode region.
r_1	Radius of electron cloud in point anode.
κT_e, κT_i	Electron and ion temperature.
t	Time.
U_e	Electron injection voltage.
$\vec{V}$	Average velocity.
$\vec{V}_0$	Velocity of the center of mass of particles.
$\vec{V}_1$	Space-and-time-perturbed velocity.
$\vec{V}_\alpha$	Average velocity of particles of species α.
$\bar{V}_{e\perp}$	Average electron velocity perpendicular to the magnetic field.
$\vec{v}$	Velocity coordinate.
$\vec{v}$	Velocity of individual particles.
$\vec{v}_p$	Phase velocity of the electromagnetic wave.
V	Plasma volume.
V	Voltage deflection on the oscilloscope.
V_{def}	Voltage reading with the plasma present.
V_{half}	Voltage reading on the oscilloscope at 90° phase angle.

LIST OF SYMBOLS (cont.)

V_{max}	Maximum voltage reading on the oscilloscope at 0° phase angle.
W_e	Electron injection energy.
$\overline{W}_{e\perp}$	Average electron energy perpendicular to the magnetic field.
x	The fraction on the total electromagnetic wave comprising the ordinary wave.
y	The fraction on the total electromagnetic wave comprising the extraordinary wave.
Y	Ratio of the electron cyclotron frequency to the frequency of the electromagnetic wave.
α_r	Effective recombination coefficient.
δ	The square of the ratio of the electron thermal speed to the wave phase velocity.
$\vec{\epsilon}$	Dielectric tensor.
ζ	Direction cosine, cos θ.
κ	Boltzmann constant.
λ	Wavelength of electromagnetic wave.
λ_p, λ_v	Wavelength of electromagnetic wave in a plasma and in a vacuum.
$\vec{\mu}$	Index of refraction.
ν_H	Diffusion rate for electrons across the magnetic field.
ν_{ve}	Diffusion rate for electrons in velocity space over the electron potential barrier.
ν_m	Ionization rate of neutral atoms.

LIST OF SYMBOLS (cont.)

ξ Direction cosine, sin θ.

ρ_m Mass density.

ρ_q Charge density of species α.

$\vec{\sigma}$ Conductivity tensor.

$\vec{\sigma}^{-1}$ Resistivity tensor.

$\sigma_{xx}, \sigma_{xy} \cdots$ Elements of conductivity tensor.

τ Confinement time.

τ_H Time required for electrons to diffuse across the

                            magnetic field.

Φ_A Applied anode-to-cathode voltage.

Φ_e, Φ_i Potential barrier heights for electrons and ions.

Φ_p Plasma potential.

$\Delta\Phi$ Magnitude of the potential depression caused by electron

                            space charge accumulation in the anode region.

ϕ Phase angle between the reference and transmission paths

                            of microwave signal in the interferometer.

ϕ_p, ϕ_v Phase angle of the microwave signal in a plasma and in

                            a vacuum.

ω Frequency of electromagnetic wave.

$\vec{\omega}_{ce}$ Electron cyclotron frequency.

ω_p Plasma frequency.

∇_r, ∇_v Gradient operators in position and velocity space.

$\perp, \parallel$ Perpendicular and parallel.

I. INTRODUCTION

The average electron density and electron confinement time of a plasma confined in an electrostatically plugged magnetic spindle cusp device is studied. A 20 GHz microwave interferometer is used to measure the electron density. A spark gap is used to pulse the electron beam and the electron density is measured as a function of time. Trends expected from theoretical equations are compared with the experimental results.

In many confinement schemes where the plasma is confined by a magnetic field in which the field lines surround the plasma smoothly, there is a tendency toward instability. The magnetic field lines, which may be thought of as being stretched around the plasma, can shorten themselves by burrowing into the plasma and forcing it outward. A confinement scheme which is stable against this type of interchange instability is one where the magnetic field lines curve away from the plasma. In order to satisfy this curvature requirement, the magnetic field configuration must possess cusps through which the field lines pass radially outward from the center of the confinement region.

The main limitation of cusp confinement schemes, which is the reason for little experimental investigation of cusps, is the high predicted plasma loss rate through the magnetic gaps in the cusp regions. There have been several proposals for reducing this loss rate. In the early 1960's, O. A. Lavrent'ev of the Soviet Union proposed the use of static electric fields in the cusp regions to

reduce the loss rate. The electric fields reflect all but the most energetic electrons and ions in the plasma. The Soviet Union has been conducting research on electrostatically plugged spindle cusp experiments[1,2,3] since the mid 1960's. Experimental devices of the type are being constructed and tested at INRS-Énergie, Université du Québec[4] and at the University of Missouri-Rolla (UMR).

Microwave diagnostics is concerned with making nonperturbing measurements of wave properties and expressing them in terms of plasma parameters. Historically, the use of microwave radiation as a diagnostic tool is not new, coming into use in the 1920's. There are two basic approaches to microwave diagnostics, active and passive. In passive wave diagnostics, if the emitted radiation can be identified and measured, then the appropriate parameters can be calculated. For example, if a high frequency oscillation is known to be due to electron plasma oscillations, then the electron density can be calculated from the plasma frequency relation. In active wave diagnostics, microwave radiation of a known frequency is transmitted through a plasma. From the effects the plasma has on the microwave radiation, appropriate parameters can be measured. Microwave interferometry belongs to this class of active wave diagnostics and will be discussed further in section III.

II. CONFINEMENT SCHEME

A. Description

The plasma confinement scheme used in this experiment is an electromagnetic cusp device. The magnetic field is produced by two magnet coils carrying current in opposite directions. The magnetic field lines emerging from the ring gap between the two coils and the two axial openings connect the interior volume of the trap with the surrounding space, Fig. 1. This type of confinement is an open magnetic system with the magnetic field strength increasing radially outward from the center of the chamber, making this confinement scheme hydromagnetically stable.

Positive and negative electrodes (anodes and cathodes) are placed at the ring cusp and the two point cusps to accomplish the electrostatic plugging. The anodes along with the chamber wall are at ground potential, while the cathodes are at a large negative potential. The electric fields created by the anode and cathode in each cusp region reflect the less energetic electrons and ions, reducing the flow of charged particles out through the magnetic gaps, thus increasing the plasma density and confinement time.

The plasma is formed by injecting an electron beam through one of the point cusps into a low pressure neutral gas. Some of the electrons from the beam will accumulate in a thin layer along the magnetic surface forming a negative space charge and potential well for the ions. Electrons from the beam will also ionize the neutral gas. Some ions will immediately be lost to the cathode, leaving
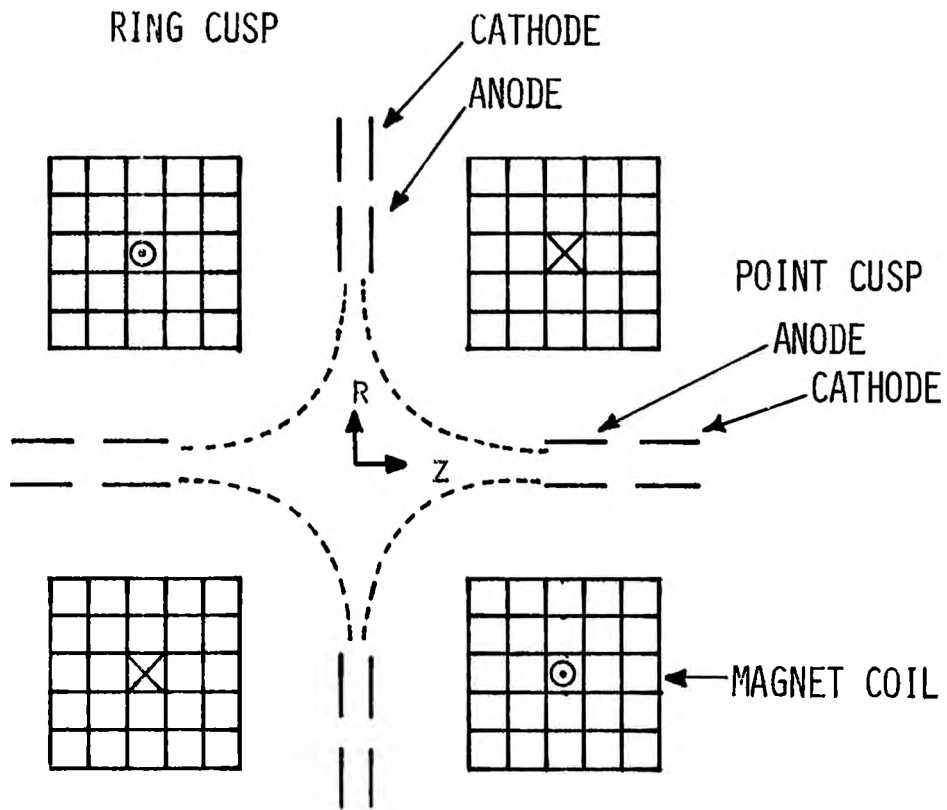
Fig. 1. Schematic Diagram of the Electrostatically
Plugged Magnetic Spindle Cusp.

additional electrons for the creation of the potential well. The magnetic field prevents the electrons from reaching the anode except by diffusion across the magnetic field lines. The potential of the cathode prevents most of the electrons from escaping along the magnetic field lines.

As the electron density in the electromagnetic trap is increased, electrons will begin to accumulate in the anode regions, partially screening the applied anode-to-cathode potential. This shielding effect reduces the applied potential by an amount proportional to the number of electrons accumulated in the anode.

A sketch of the electrostatic potential along the z-axis is shown in Fig. 2. The dashed curve represents the initial potential distribution in the absence of a plasma and the solid curve represents the potential in the presence of plasma. The applied potential between the anode and cathode is Φ_A. The potential barriers "seen" by the positive ions and electrons are Φ_i and Φ_e, respectively. The potential depression in the anodes caused by the accumulation of electrons in the anode regions is $\Delta\phi$ and is discussed further in the next section. The radial potential distribution in the midplane has a similar shape. Therefore, the plasma is confined by the combined electric and magnetic fields and by the space charge field of the plasma itself.

B. Limitations

There are several limitations to the confinement of a plasma. The first of these is the limitation of the reflection of charged
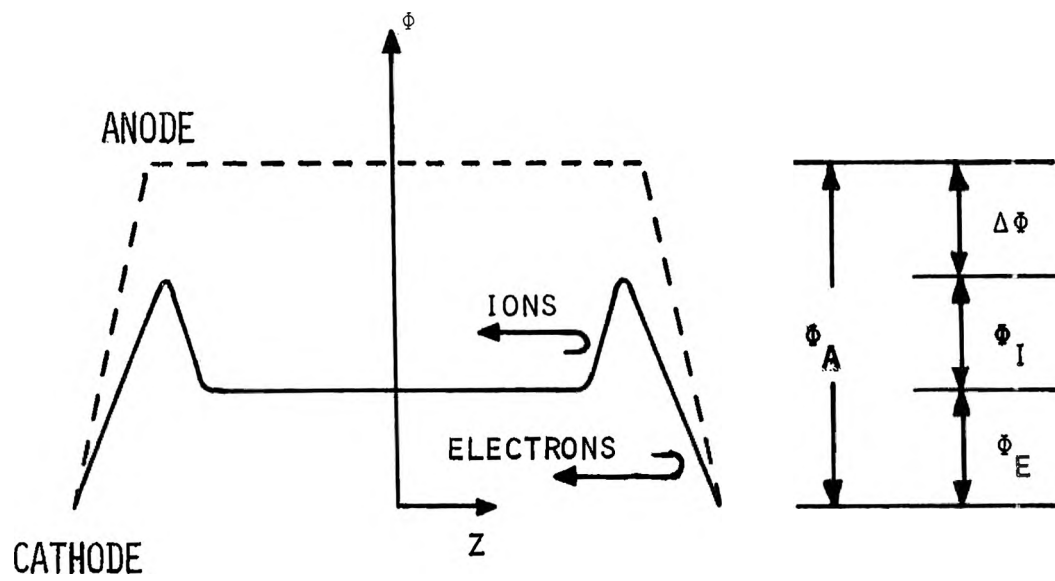
Fig. 2. Axial Variation of the Electrostatic Potential Φ.

particles from the plasma by the magnetic field. When the plasma is reflected, the magnetic field is displaced outward until the magnetic field pressure is equal to the plasma kinetic pressure. In order for the magnetic confinement to be effective, the plasma pressure must be less than the magnetic pressure at the surface of the chamber, otherwise, the magnetic field will be completely displaced from the chamber volume causing the plasma to come into contact with the wall.

As mentioned earlier, the electromagnetic cusp confinement scheme is hydromagnetically stable. However, there is an instability, called the diocotron instability, occurring in the ring anode gap. It results from the large electron density gradient and strong electric field found there. The diocotron instability grows on the accumulated cold electrons formed by ionization of the neutral gas in the magnetic gap. The electrons in the ring anode gap undergo an $\vec{E} \times \vec{B}$ drift in the azimuthal direction around the ring gap due to the applied electric and magnetic fields. The velocity of the drifting electrons increases toward the outer edges of the electron layer. This slipping or shear in the electron flow, moving in opposite directions about the ring anode centerline, causes the onset of the diocotron oscillation. The shear in the electron flow causes small ripples or oscillations in the flow which sets up a secondary drift of electrons toward the anode walls. This secondary drift can lead to plasma loss. The diocotron oscillation can be stabilized. Some of the methods for stabilization are: a) move the electron layer closer to one anode wall by varying the magnetic field in each half of the trap[3], b) decrease the size of the anode gap and c) apply a larger negative potential to the

cathode[4].

The dioctron instability can be beneficial by reducing the
potential depression in the ring anode. This is accomplished by
removing the cold electrons. The cold electrons have two degrading
effects on the plasma and its confinement. First, the cold electrons
reduce the average electron temperature. Secondly, the accumulation
of electrons in the anode increases the potential depression, which in
turn reduces the density of confined electrons. This is discussed
below.

In experimental work done in the Soviet Union, the suppression
of the diocotron oscillation resulted in an increase in plasma density
from 10^8 to $2-5\times10^{11}$ cm^{-3} [3].

A third limitation is caused by the accumulation of electrons in
the point and ring cusp anode regions. The electron space charge in
the anode depresses the applied potential Φ_A by an amount $\Delta\Phi$, see
Fig. 2. If $\Delta\Phi$ becomes too large, the electrostatic confinement ceases
to be effective. Ware and Faulkner[5] calculated the maximum electron
density which can be confined in the cusp anodes. They assumed a
triangular distribution function for each cusp region centered about
the r and z-axis with a maximum density of n_A on the axis. The radius
of the electron cloud is assumed to be 2 Larmor radii (r_L) in the ring
anode and 20 Larmor radii in the point cusp[5]. For a potential
depression of $\Delta\Phi$, their results are, in Gaussian units,

$$(n_A)_{ring} = \frac{\Delta\Phi}{2\pi ed_1 [a_r - \frac{1}{3} d_1]} \text{ cm}^{-3} \qquad (2-1)$$

$$(n_A)_{\text{point}} = \frac{\Delta\Phi}{\pi e r_1^2 [\frac{5}{9} + \frac{2}{3} \ln(\frac{a_p}{r_1})]} \text{ cm}^{-3} \qquad (2\text{-}2)$$

where r_1 is the radius of the electron cloud and a_p is the radius of the gap in the point cusp region, d_1 is the half-width of the electron cloud and a_r is the half-width of the gap in the ring cusp region, e is the electronic charge in esu. The potential depression, $\Delta\Phi$, is less than or approximately equal to the applied voltage. The average electron Larmor radius is given as

$$r_L = \frac{\overline{V}_{e\perp}}{\omega_{ce}} = \frac{c(2m\overline{W}_{e\perp})^{1/2}}{eB_0} = \frac{3.37(\overline{W}_{e\perp} \text{ [eV]})^{1/2} \text{ cm}}{B_0 \text{ [Gauss]}} \qquad (2\text{-}3)$$

where $\overline{V}_{e\perp}$ and $\overline{W}_{e\perp}$ are the average electron velocity and the average electron energy perpendicular to the magnetic field, c is the speed of light, m is the electron mass, B_0 is the applied external magnetic field, and ω_{ce} is the electron cyclotron frequency defined as

$$\omega_{ce} = \frac{e\vec{B}_0}{mc} = 1.76 \times 10^7 B_0 \text{ [Gauss] radians/sec}$$

The accumulation of electrons in the anodes effectively shields the applied electric potential and thus limits the density obtainable in the central plasma region. Moir, Barr and Post[6] calculated the ratio of the electron density in the anode to the density in the central plasma region to be

$$\frac{(n_A)_{\text{point}}}{n_e} = e^x (1 - \text{erf } x^{1/2}) \qquad (2\text{-}4)$$

where $x = e\Phi_i/\kappa T_e$. The energy an ion would need to penetrate the potential barrier Φ_i is $e\Phi_i$ and κT_e is the electron temperature in the anode region. Since electrons near the anode surface are accelerated by the potential difference $\Phi_i + \Delta\Phi$, the electron temperature, κT_e, should be replaced by $\kappa T_e + e(\Phi_i + \Delta\Phi)$. The average electron energy perpendicular to the magnetic field is $\overline{W}_{e\perp} \simeq \kappa T_e$, while in the anode region $\overline{W}_{e\perp} \simeq \kappa T_e + 2/3(e\Phi_i + e\Delta\Phi)$.

Many of the parameters used are based on Soviet experimental values[7] except for values of $\Delta\Phi$ and r_1. Lavrent'ev[1] indicated in his discussion of the electron density in the ring cusp region that the best confinement occurred when the potential depression was 0.2 to 0.3 times the electron injection voltage, U_e. Nothing was mentioned about the magnitude of the potential depression in the point cusp region. From Fig. 2, it is obvious that $\Delta\Phi \leq \Phi_p$, the plasma potential where $\Phi_p = \Delta\Phi + \Phi_i$. The experimental parameters for the Soviet Jupiter 1M experiment indicates $\Phi_p \simeq 0.5$ to $0.6\ U_e$ while $\Delta\Phi = 0.5\ U_e$ was assumed for this experiment. Osher[7] and Lavrent'ev[1] indicated that for the Soviet results $\Phi_p \rightarrow U_e$ when the pressure exceeded 10^{-6} Torr.

There is general agreement that the radius of the electron cloud in the ring anode is about $2r_{Lr}$[1,2,5] where r_{Lr} is the Larmor radius in the ring anode. Matching magnetic field lines between the ring and point anodes, the electron cloud radius in the point cusp is $r_1 = 2(Rr_{Lp})^{1/2}$ where R is the radius of the ring anode and r_{Lp} is the Larmor radius in the point anode. Ware and Faulkner[5], on the other hand, suggest a typical value for $r_1 \simeq 20r_{Lp}$ which is about 1/5 of

$2(Rr_{Lp})^{1/2}$. A value of $r_1 = 20r_{Lp}$ was assumed for this experiment along with the approximation $\Delta\Phi = 0.5\ \Phi_A$.

In this experiment, the applied potential, Φ_A, is the same as the electron injection voltage, U_e, and not equal to the more negative potentials applied to the other cathodes. The reason for this is that the electrons will escape through the magnetic gap with the smallest applied potential.

Using Eqs. (2-1) to (2-4), an approximate electron density can be calculated for this experiment. Listed In Table I are typical operating parameters for the UMR experiment. Substituting the parameters into Eqs. (2-1) and (2-2), the electron densities obtained for the ring and point anode regions are 2.0×10^{10} and 0.84×10^{10} cm^{-3}, respectively. The point anode has the smaller of the two density values and thus it is the limiting anode in confining the plasma. Equation (2-4) gives a density in the central plasma region of 1.5×10^{10} cm^{-3}.

In order to obtain a complete theoretical description of the plasma parameters (electron and ion temperature and density, the potential depression in the cusp anode regions, and the electron and ion potential barriers), a set of nonlinear and algebraic equations which depend on the externally applied magnetic field, the electron injection energy and current, the pressure and the applied anode-to-cathode voltage must be solved. Until this problem has been solved, we are limited to approximate mathematical equations and noting trends in the relation between various parameters obtained from previous experimental work.

TABLE I. Typical Operating Parameters for the UMR Experiment.

Electron injection voltage: U_e = 500 V

Electron injection energy: W_e = 500 eV

Base pressure: p = 10^{-6} Torr

Operating pressure: p = 10^{-5} Torr

Magnetic induction

    ring cusp: B_r = 3000 Gauss

    point cusp: B_z = 5000 Gauss

Ring gap half-width: a_r = 0.38 cm

Point gap radius: a_p = 0.7 cm

Empirical relations assumed:

Electron cloud radius

    ring cusp: d_1 = 2 r_{Lr} cm[5]

    point cusp: r_1 = 20 r_{Lr} cm[5]

Electron temperature: $\kappa T_e \simeq 0.15\ W_e$ eV[8]

Ion temperature: $\kappa T_i \simeq 0.12\ W_e$ eV[6,8]

Potential depression in the anode: $\Delta\Phi \simeq 0.5\ \Phi_A$ statvolt*

Plasma potential: $\Phi_p \simeq 0.6\ \Phi_A$ statvolt[6]

Ion potential: $\Phi_i \simeq \Phi_p - \Delta\Phi$ statvolt


*1 statvolt = 300 Volts

III. EXPERIMENTAL CONSIDERATIONS

A. Electromagnetic Cusp Experiment

Figure 3 is a photograph of the experiment and Table II lists pertinent information regarding the major components of the experiment. The chamber, constructed of 304 and 316 stainless steel, is cyclindrical in shape. It has eight diagnostic ports and two ports for the point cusp electrodes and electron gun, see Fig. 4. Hollow copper wire wound around each half of the chamber and two end coils which fit over the point cusp ports comprise the coils. Two arc welders supply approximately 600 amperes of current to each of the coils. 600 amperes of current is equivalent to a magnetic induction of approximately 3000 Gauss in the ring cusp and 5000 Gauss in the point cusp. Figure 5 is a plot of the magnetic field lines and surfaces of constant magnetic induction generated by the computer code MAFCO[8] for 600 amps through the coils. Using the innermost magnetic field lines as the plasma boundary, the plasma volume and surface area are found to be 469 cm^3 and 1584 cm^2.

The coils are water-cooled to prevent overheating. The cooling system is a closed loop cycle. Water is pumped from a 1 cubic meter tank through the coils under $2.8x10^6$ dyne/cm^2 (40 psi) pressure and returns through a large heat exchanger to the tank. Four fans are placed above the heat exchanger to improve the cooling capacity of the system.

Also shown in Fig. 5 is the relative size and location of the point and ring cusp electrodes. The point cusp electrodes are
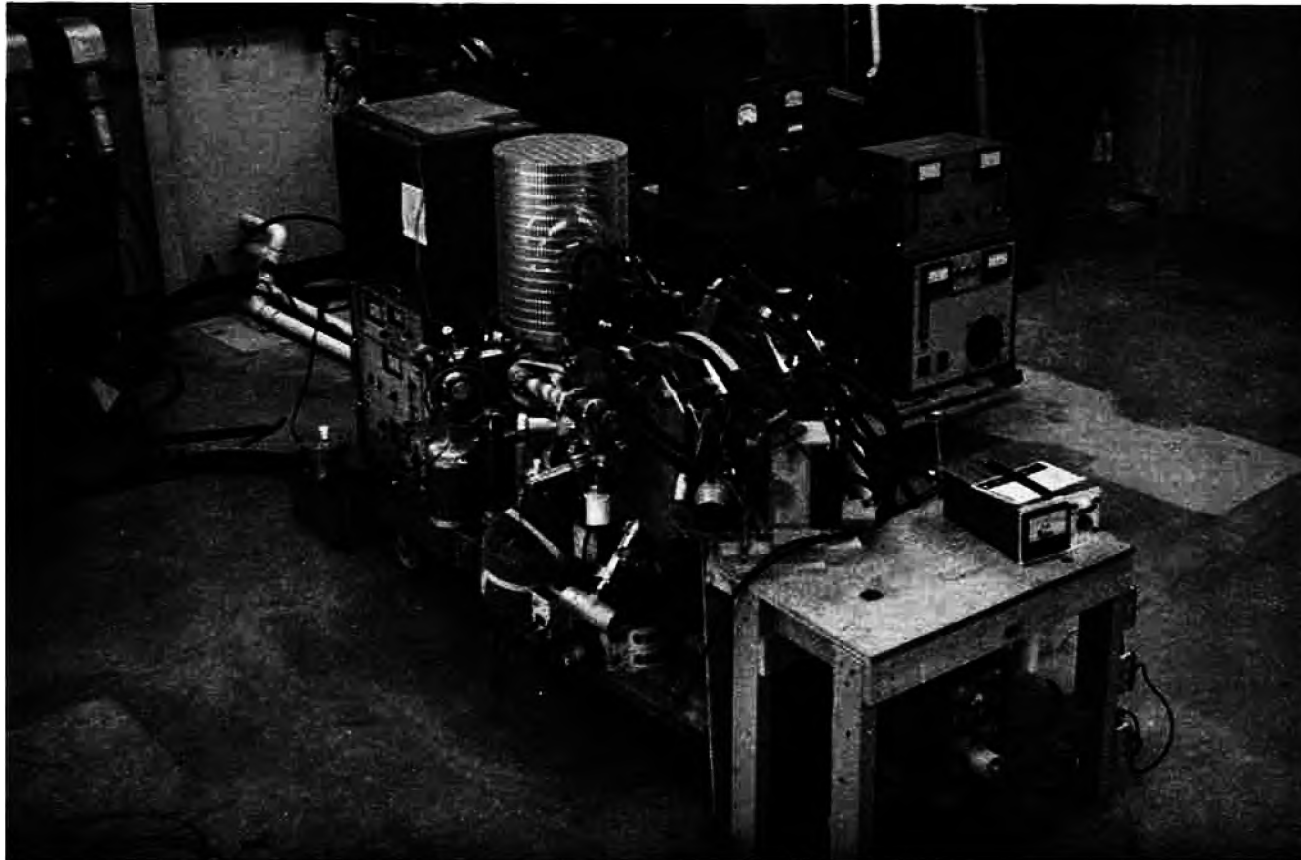
Klystron, wavemeter, 360° phase shifter and variable attenuator
are setting on the table in front of the experimental device.

Fig. 3. Photograph of the Electromagnetic Cusp Experiment.

TABLE II. Pertinent Information on Major Components
of the UMR Experiment.

CHAMBER

inside diameter: 24.6 cm

inside length: 17.8 cm

number of diagnostic ports: 8

inside diameter of ports: 3.4 cm

MAGNET SYSTEM

magnet coil wire: copper

cross-sectional area: 0.8 cm^2

center hole cross-sectional area: 0.5 cm^2

cooling system: water under 40 psi pressure

current source: 2 arc welders

rated: 1000 amps at 50 volts

obtainable: 600 amps at 50 volts

coil resistance: 0.083 Ω

magnetic field strength obtainable at 600 amps

point cusp region: ∿5000 Gauss

ring cusp region: ∿3000 Gauss

VACUUM SYSTEM

dry-vane mechanical pump

vacuum obtainable: ∿20 Torr

liquid nitrogen cryosorption pump

vacuum obtainable: ∿10^{-3} Torr

ionization pump

vacuum obtainable: $\lesssim 10^{-7}$ Torr

TABLE II. (cont.)

base pressure in chamber: $\lesssim 10^{-6}$ Torr

total conductance of connecting tubes: ~ 12 liter/sec.

ELECTROSTATIC PLUGGING SYSTEM

    point cusp electrodes, anode and cathode

        inside diameter: 1.4 cm

        length: 3.0 cm

        separation between electrodes: 1.3 cm

    ring cusp electrodes

        anode gap width: 0.76 cm

        anode radius: 16.1 cm

        cathode: 0.8 cm diameter hollow steel ring

        cathode radius: 17.8 cm

ELECTRON GUN

    filament: directly heated thoriated tungsten wire mesh

        maximum output current: ~ 10 milliamps

    anode and grid: same dimensions as other point cusp electrodes

        separation between anode and grid: 1.3 cm

    cathode: flat circular disk placed approximately 0.3 cm

        behind filament

DIAGNOSTIC
PORTS

MAGNET COILS

POINT CUSP

ANODE

CATHODE

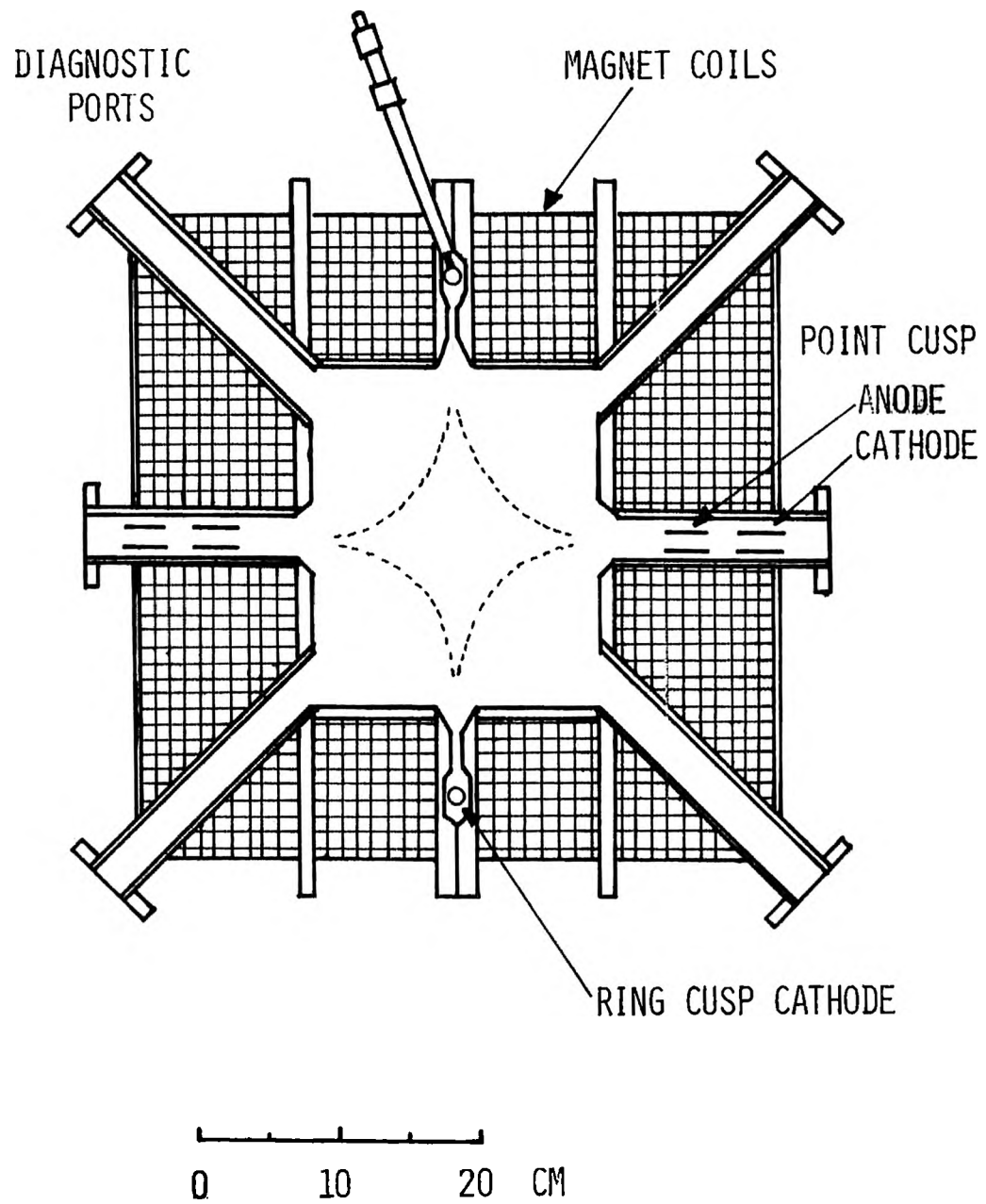RING CUSP CATHODE

0   10   20   CM

Fig. 4. Schematic Diagram of the Electromagnetic Trap Showing
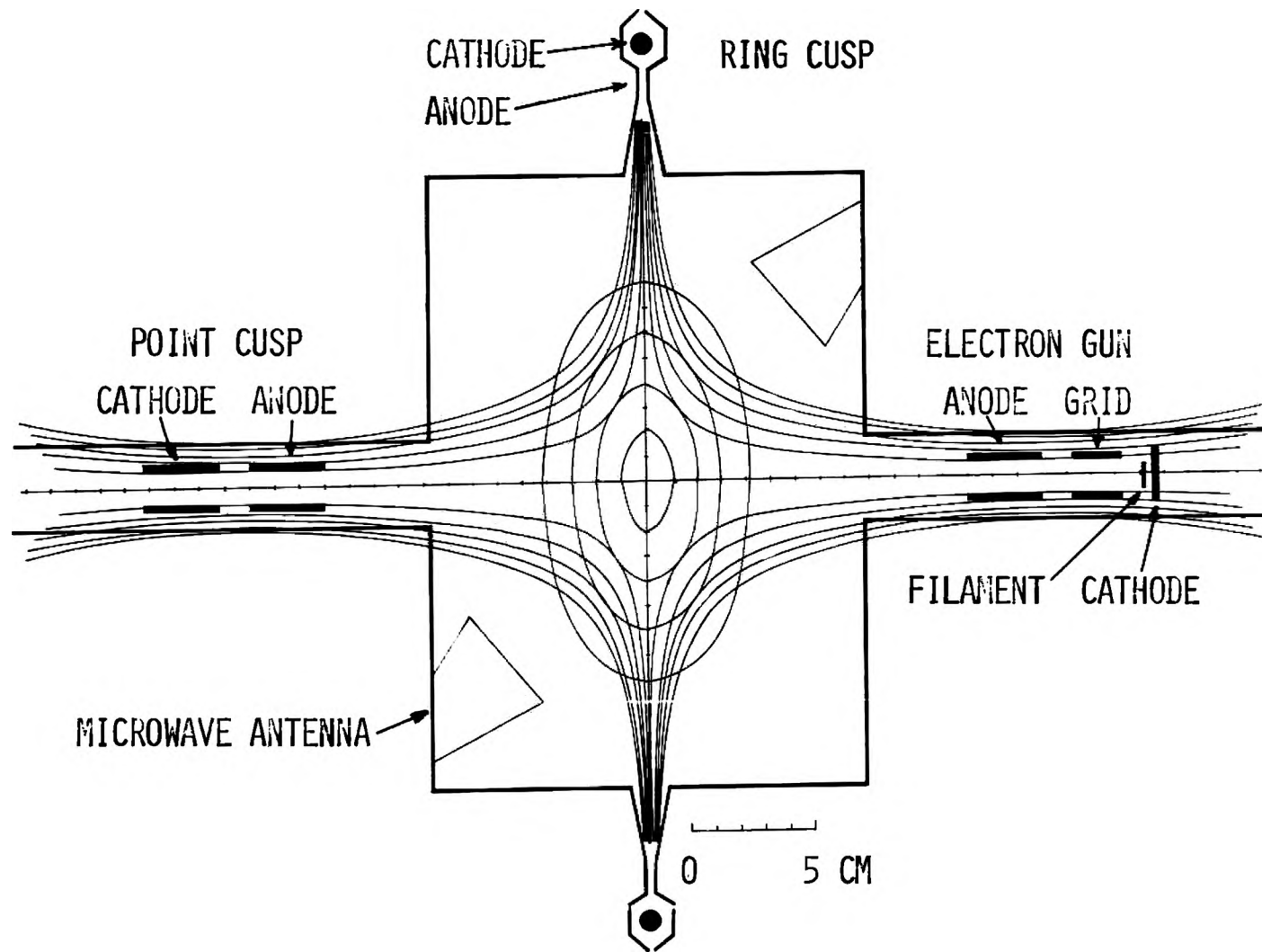Location of Diagnostic Ports and Cusp Electrodes.

Fig. 5. Magnetic Field Lines and Surfaces of Constant Magnetic Induction for the Electromagnetic Trap.

hollow cylinders. A gap in the wall where the flange of the two

chamber halves fit together forms the ring cusp anode. A hollow

steel loop, resting on four insulating posts outward from the

anode gap, forms the ring cusp cathode. Nominal operating voltages

for the point cusp cathode are -5 to -7 kilovolts and -5 kilovolts

for the ring cusp cathode.

The electron gun consists of a cylindrically shaped anode and

grid in front of the filament. The grid is used to pulse the

electron beam. The filament of the electron gun is directly

heated by its own power supply. Increasing the current through the

filament increases the thermionic emission current from the filament.

The electron injection voltage is supplied by a separate power

supply. Thus, the electron beam current can be varied while

maintaining a constant injection voltage.

B. Operation of the Microwave Interferometer

A schematic of the experimental arrangement is illustrated in

Fig. 6. The components of the microwave interferometer are:

klystron, variable attenuator, wavemeter, tunable waveguide tee,

transmitting and receiving antennas, tunable detector, variable

attenuator, 360° phase shifter, $\overrightarrow{EH}$ tuner, and klystron power supply.

Upon leaving the klystron, the microwaves are split into two

paths. In one, which is referred to as the transmission path, are

the transmitting and receiving antennas. In the other, referred to

1. KLYSTRON, VARIABLE ATTENUATOR
   AND WAVEMETER
2. TRANSMITTING AND RECEIVING
   ANTENNA
3. TUNABLE DETECTOR
4. 360 ° PHASE SHIFTER
5. VARIABLE ATTENUATOR
6. $\overset{\rightrightarrows}{\text{EH}}$ TUNER
7. KLYSTRON POWER SUPPLY
8. OSCILLOSCOPE
9. POINT AND RING CATHODE H.V.
   POWER SUPPLY
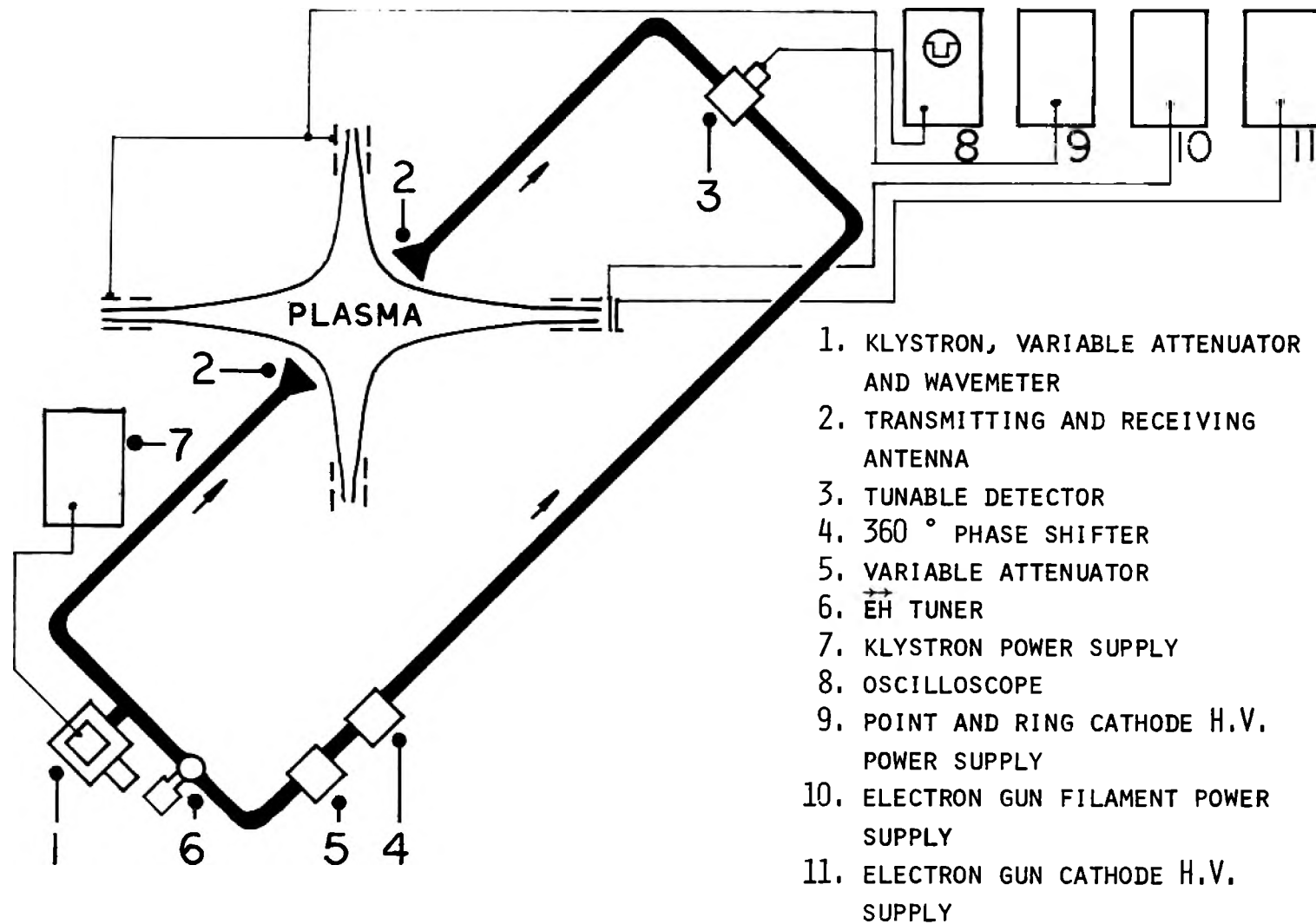10. ELECTRON GUN FILAMENT POWER
    SUPPLY
11. ELECTRON GUN CATHODE H.V.
    SUPPLY

Fig. 6. Schematic Diagram of the Microwave Interferometer.

as the reference path, are the phase shifter, attenuator and $\overset{\rightarrow\rightarrow}{EH}$ tuner.
The latter, along with the tuning stub on the detector, are adjusted
so the reference wave interferes destructively with the transmitted
wave yielding a null output in the absence of a plasma. When a
plasma of sufficient density is present in the transmission path, a
shift in phase occurs which unbalances the circuit. The resulting
output is recorded on the oscilloscope.

The operation and service manual for the Hewlett Packard 715A
Klystron Power Supply[9] describes the controls and their functions,
and the general operation of the power supply and reflex klystron. The
klystron generates a 20.0 GHz signal and is tunable over a frequency
range of approximately ±10%. Knowing the frequency of operation of
the klystron is more important than tuning the klystron for a
particular frequency.

The correct procedure for energizing the klystron is described
in Ref. [10]. With the klystron modulated at 1 kHz, the reflector
voltage can be adjusted to give a rectangular pulse shape. Having
tuned the klystron for maximum power at the desired frequency, the
reference path of the interferometer is tuned so the reference wave
will interfere destructively with the transmitted wave. The
attenuator varies the amplitude of the wave in the reference path to
match the amplitude of the wave in the transmission path. The phase
shifter varies the phase of the reference signal through 360°. The
$\overset{\rightarrow\rightarrow}{EH}$ tuner and the tuning stub at the detector act as a phase shifter.
When the amplitudes are matched and the tuners are adjusted properly,
the detector signal can be nulled with the phase shifter making

$\phi = 180°$ where ϕ represents the phase angle between the waves from the two arms of the interferometer. Reference [11] gives a more complete description of the microwave components.

Upon completing the above adjustments, a 1 kHz rectangular wave pulse with some given maximum amplitude at $\phi = 0°$ should be seen on the oscilloscope. If the tuning stub on the phase shifter is rotated, the amplitude of the 1 kHz signal will decrease smoothly to zero, $\phi = 180°$. Continued rotating of the tuning stub will again increase the amplitude of the pulse to the same maximum value, $\phi = 360°$. Slight readjustment of the modulation or reflector voltage may be necessary to maintain a consistent maximum signal amplitude and a clean rectangular pulse shape.

Plotting the amplitude of the signal obtained from the scope versus the phase angle ϕ introduced by the phase shifter, the plot in Fig. 7 is obtained. The equation for this curve is

$$V = \frac{V_{max}}{2}(1 + \cos \phi).$$

The equation can be solved for ϕ in terms of the voltage readings obtained from the scope.

The procedure for obtaining data is as follows: First, the magnetic field is energized and the maximum amplitude of the microwave signal is recorded. The phase shifter is adjusted so the amplitude is approximately half the maximum. The reason for doing this is that any phase shift about $\phi \simeq 90°$ (see Fig. 7) will appear as a larger deflection on the scope than would the same phase shift
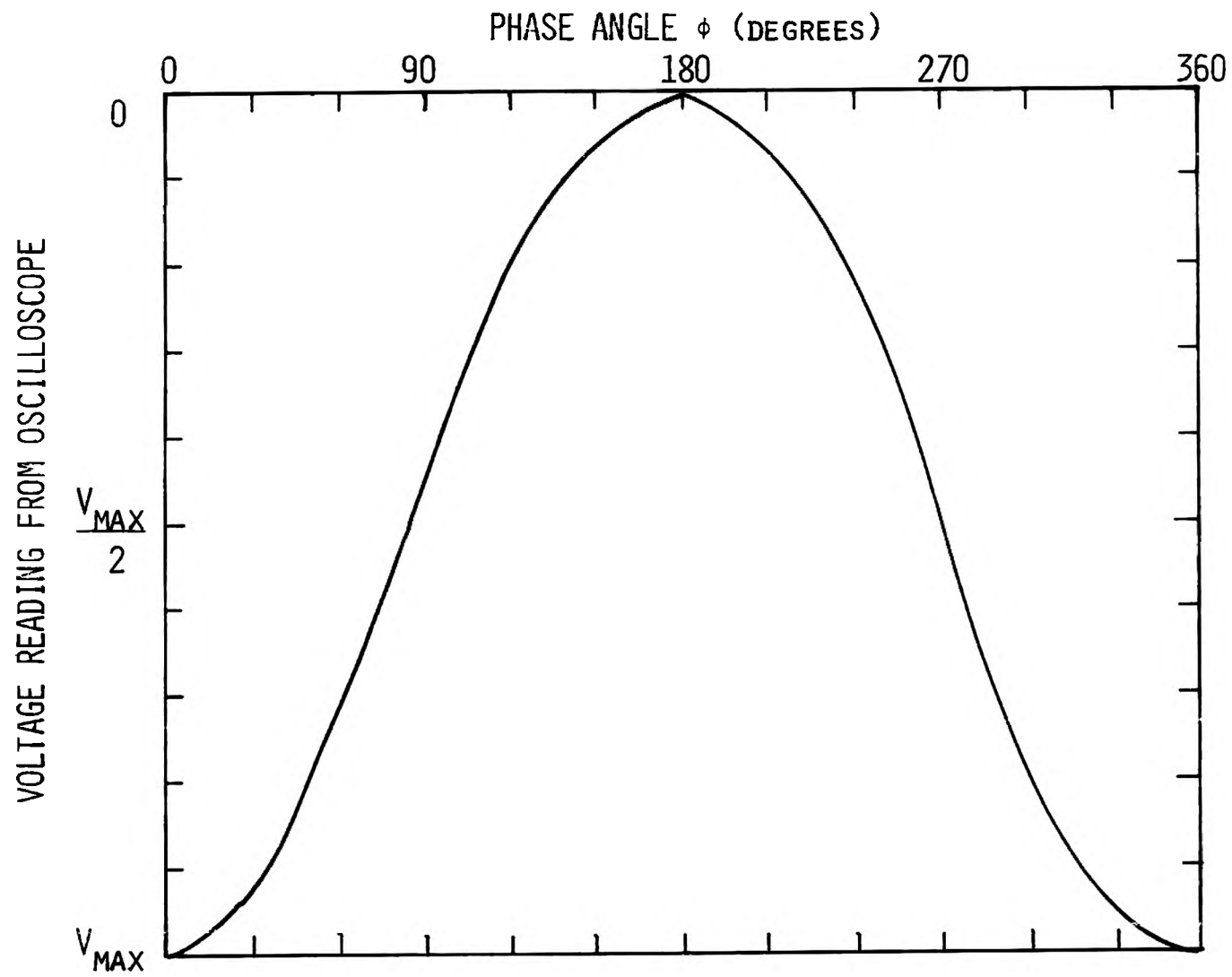
Fig. 7. Oscilloscope Voltage Variation as a Function of Phase Angle.

about $\phi \approx 0°$ or $180°$. Next, the electron beam is energized, producing a plasma, which causes the amplitude of the signal to change. This value is also recorded. Several readings are then taken with the plasma alternately turned "on" and "off" and then averaged. Finally, the maximum deflection is measured again and averaged with its initial value, since it may drift a few percent.

Thus, a maximum reading V_{max}, a reading at approximately half the maximum V_{half} with no plasma present and a reading with the plasma present V_{def} are obtained. With these readings, the phase angle for the microwaves in a vacuum and in a plasma can be found from,

$$\phi_v = \text{Arc } \cos(\frac{2V_{half}}{V_{max}} - 1) \qquad (3\text{-}1)$$

$$\phi_p = \text{Arc } \cos(\frac{2V_{def}}{V_{max}} - 1). \qquad (3\text{-}2)$$

The difference between the two phase angles gives the phase shift $\Delta\phi$ due to the plasma,

$$\Delta\phi = -(\phi_p - \phi_v). \qquad (3\text{-}3)$$

Appendix A describes the operation of the confinement device while Appendix B describes some of the major problems encountered in operating the experimental device.

C. Microwave Interferometer Phase Shift-Electron Density Relation

To use the microwave interferometer effectively as a diagnostic

tool, a relationship between the frequency of the microwave signal, the wavelength of the signal in the plasma and the electron density must be determined. This relationship is called a dispersion relation and is derived in Appendix C. For an electromagnetic wave propagating through a vacuum this relation is $k_v = \omega/c$ where k_v ($= 2\pi/\lambda_v$), λ_v and ω are the wave number, wavelength and the frequency of the electromagnetic wave. A subscript p on k, λ and ω indicate quantities in reference to the plasma. The speed of light, c, is the phase velocity, v_p, of an electromagnetic wave propagating through a vacuum.

Because of the alignment of the microwave antennas with the magnetic field, only propagation perpendicular to the magnetic field, $\theta = 90°$, needs to be considered. The waveguide is situated so the electric field vector, $\vec{E}$, of the electromagnetic wave is parallel to the external magnetic field $\vec{B}_0$. Actually the wave propagation, $\vec{k}$, is not always perpendicular to $\vec{B}_0$ and a general case is discussed in Appendix D. This particular alignment of the electromagnetic wave with the magnetic field is referred to as the "ordinary wave" because it has the same dispersion relation as if no external magnetic field were present. The dispersion relation for the ordinary wave is derived in Appendix C and is repeated as

$$k_p^2 = (\omega^2/c^2)[1 - (\omega_p/\omega)^2] \tag{3-4}$$

where

$$\omega_p = \left(\frac{4\pi n_e e^2}{m}\right)^{1/2} = 5.64 \times 10^4 (n_e)^{1/2} \text{ radians/sec} \tag{3-5}$$

is referred to as the plasma frequency, n_e is the electron density, m is the electron mass and e is the electronic charge in esu.

Figure 6 illustrates the experimental arrangement of the microwave interferometer. The signal in the reference path is adjusted for a null output at the detector in the absence of a plasma. When a plasma is present, the wavelength of the signal, and thus its phase through the plasma, are changed and the signal at the detector is no longer zero.

The phase constants for a vacuum and plasma of thickness L are

$$\phi_v = 2\pi \left(\frac{L}{\lambda_v}\right) = k_v L \text{ radians}$$

and $$(3\text{-}6)$$

$$\phi_p = 2\pi \left(\frac{L}{\lambda_p}\right) = k_p L \text{ radians.}$$

The phase advancement introduced by the plasma in the transmission path becomes

$$\Delta\phi = -\int_0^L (k_p - k_v) \, dx. \qquad (3\text{-}7)$$

Substitute Eq. (3-4) and the expression for k_v into Eq. (3-7) to obtain

$$\Delta\phi = \frac{\omega}{c} \int_0^L [1 - (1 - \frac{n_e(x)}{n_c})^{1/2}] \, dx$$

where $n_c = (\omega^2 m/4\pi e^2)$ corresponds to a critical density associated with the signal frequency ω and defined by the plasma frequency

relation and $n_e(x)$ is the electron density at a position x along the transmission path. If $n_e(x)$ at any point along the transmission path becomes greater than n_c, the microwave signal will be cut off. To first order in $n_e(x)/n_c$,

$$\Delta\phi \simeq \frac{\omega}{2cn_c} \int_0^L n_e(x) \ dx. \qquad (3-8)$$

An average electron density over the path L can be defined as

$$\bar{n} = \frac{\int_0^L n_e(x) \ dx}{L} \ ,$$

Solve Eq. (3-8) for the integral and substitute this into the above equation to obtain

$$\bar{n} = \frac{mc}{e^2} \frac{\Delta\phi}{L}(\frac{\omega}{2\pi})$$

or

$$\bar{n}[cm^{-3}] = 118.4 \ \frac{(\omega/2\pi) \ [Hz] \Delta\phi \ [rad]}{L \ [cm]} \ . \qquad (3-9)$$

Equation (3-9) is the desired relation between the average electron density, the frequency of the microwave signal, the thickness of the plasma and the measured phase shift.

IV. RESULTS

A. Discussion of Errors

The average electron density is found from Eq. (3-9). The microwave frequency is determined from the wavemeter in the interferometer. The path length is approximated from Fig. 5 and the phase shift is obtained experimentally as described in section III-B.

The error bars are quite large, typically about $\pm 1.3 \times 10^{10} \text{ cm}^{-3}$, which is about 50% of the largest values. The error in the electron density is given by the equation

$$\frac{\delta n_e}{n_e} = [(\frac{\delta \Delta \phi}{\Delta \phi})^2 + (\frac{\delta L}{L})^2]^{1/2}$$

where δ represents the error in a reading.

The plasma thickness, as measured from the magnetic field line plot of Fig. 5, is approximately 7 cm with an error of ± 1.5 cm. The error in reading the oscilloscope is ± 1 mm, whereas, the maximum deflection of the signal as compared with the reference (no plasma) signal is approximately 3 mm. Using Eqs. (3-1) through (3-3), it is found that the phase shift varies from about 1 degree to 6 degrees.

Thus, it can be seen that the largest contribution to the error is the small voltage deflection on the oscilloscope. Increasing the amount of the deflection will reduce the size of the error. This can be accomplished by using a lower frequency interferometer or, preferably, by increasing the plasma density through modifications to the experiment.

B.   Electron Confinement Time

The plasma confinement time is closely related to the electron "e-folding time" or electron confinement time which can be measured. There are several mechanisms by which plasma can be lost from the electromagnetic trap. Electron-ion recombination need not be considered for this experiment. The diocotron instability does not seem to lead to rapid plasma loss[3,12]. The electron energy distribution function in the plasma is truncated at the electron potential barrier height $e\Phi_e$, thus, electrons can be lost by diffusion in velocity space over the potential barrier. The same mechanism leads to loss of ions.

Electrons can also be lost by diffusion across the magnetic field due to collisions of the electrons with other particles. (This loss mechanism has been neglected in cusp geometries since the loss rate through the cusp openings was much greater. However, with electrostatic plugging in the cusp regions, the cusp losses have been greatly reduced.) For this device, the principle loss mechanism is classical diffusion, the diffusion across the magnetic field lines due to electron-neutral atom collisions.

A high voltage spark gap switch was used to pulse the grid of the electron gun. A continuous injection of electrons is required to maintain the electron space charge by replacing those electrons lost from the trap. When pulsing the electron gun on and off, the electron density can be measured as a function of time from the interferometer signal displayed on the oscilloscope. From this information, the confinement time for electrons can be determined. Data were taken at

a pressure of 10^{-5} Torr hydrogen gas. The magnetic induction in the point cusp was 5030 Gauss and the electrons were injected into the trap with energies of 500, 600, 750 and 1000 eV. Figures 8 and 9 illustrate the results of this experiment. The time required for the electron density to decrease by a factor of e is a measure of the electron confinement time. For injection energies of 500, 600, 750 and 1000 eV, the corresponding experimental confinement times for electrons are 80, 115, 93 and 37 µsec. The largest error is 20 µsec. These data points are plotted in Fig. 10.

The diffusion time for the UMR experiment is approximated as[12]

$$\tau_H = (\frac{r_{Lmax}^2}{r_L})/(5.9 \times 10^{-9} p) \text{ sec} \tag{4-1}$$

where p is the background gas pressure. The diffusion across the magnetic field lines occurs most rapidly in the ring anode region because of the small dimensions. Thus, r_L is the Larmor radius in the ring gap and r_{Lmax} is the distance between the centerline in the ring anode and the magnetic flux line that grazes the anode surface. This flux line is determined from the field lines in the point anode. From the magnetic field line data in Fig. 5, it is found that $r_{Lmax} = 0.05$ cm.

The theoretical diffusion time, τ_H, is plotted as a function of electron injection energy in Fig. 10 for comparison with the experimental values of the electron confinement time. The agreement between theory and experiment is within 65%.

$P = 1 \times 10^{-5}$ Torr (H_2)

$B_Z = 5030$ Gauss

● $W_E = 1000$ eV, $\tau_E = 37 \,^{+18}_{-10}$ μSEC

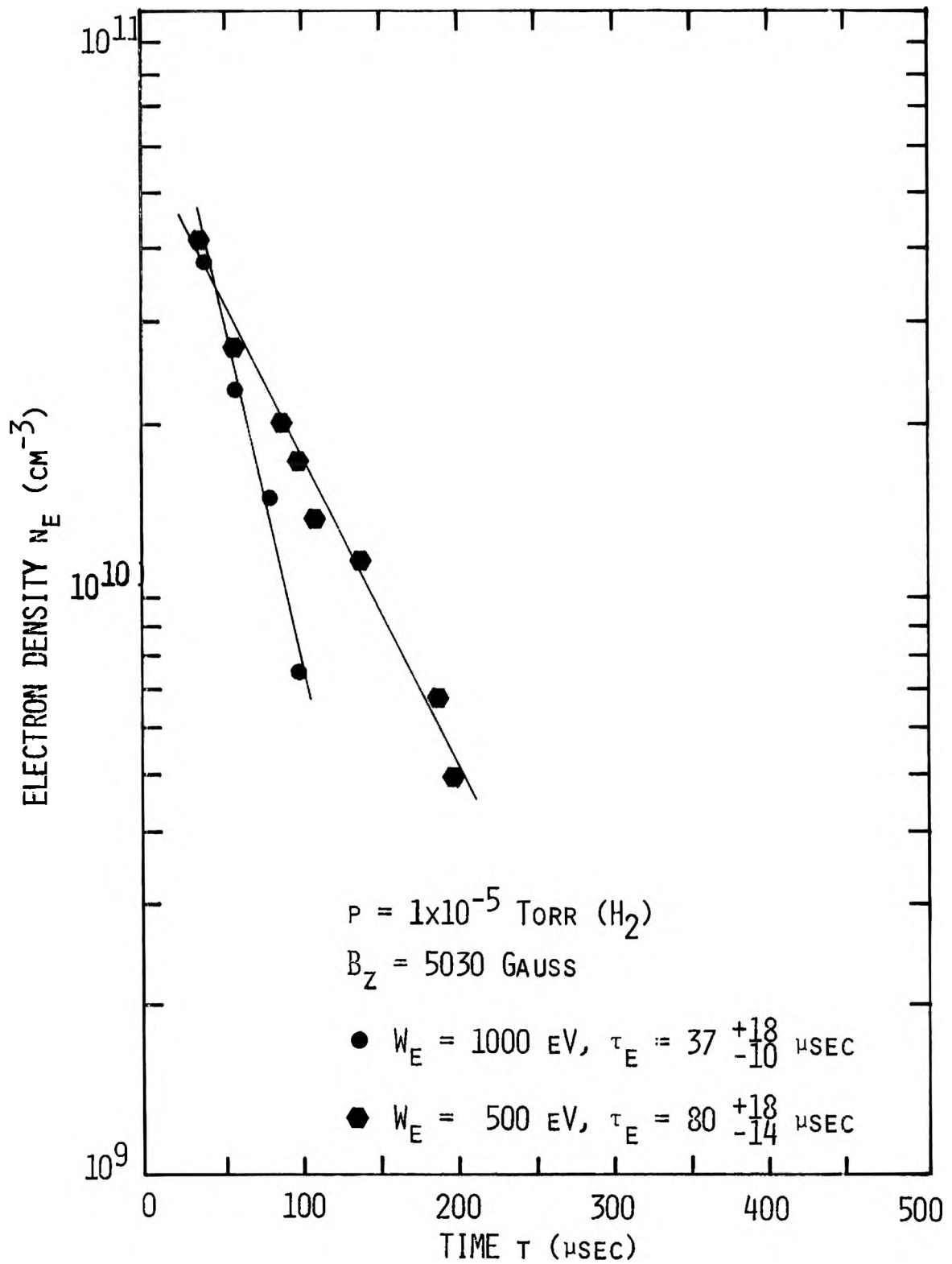⬢ $W_E = 500$ eV, $\tau_E = 80 \,^{+18}_{-14}$ μSEC

Fig. 8.   Time-Decay of Electron Density at
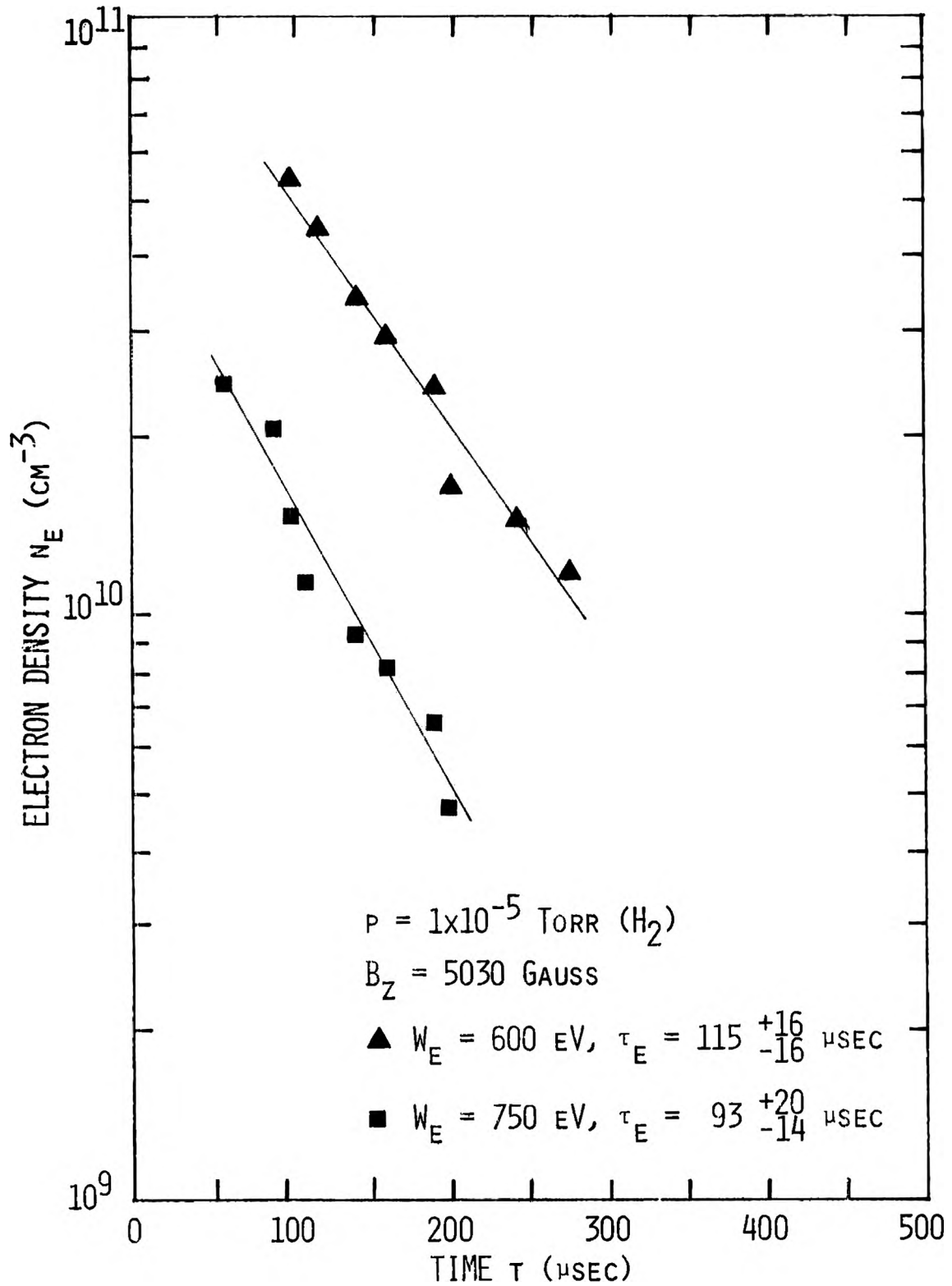Injection Energies of 500 and 1000 eV.

Fig. 9.   Time-Decay of Electron Density at
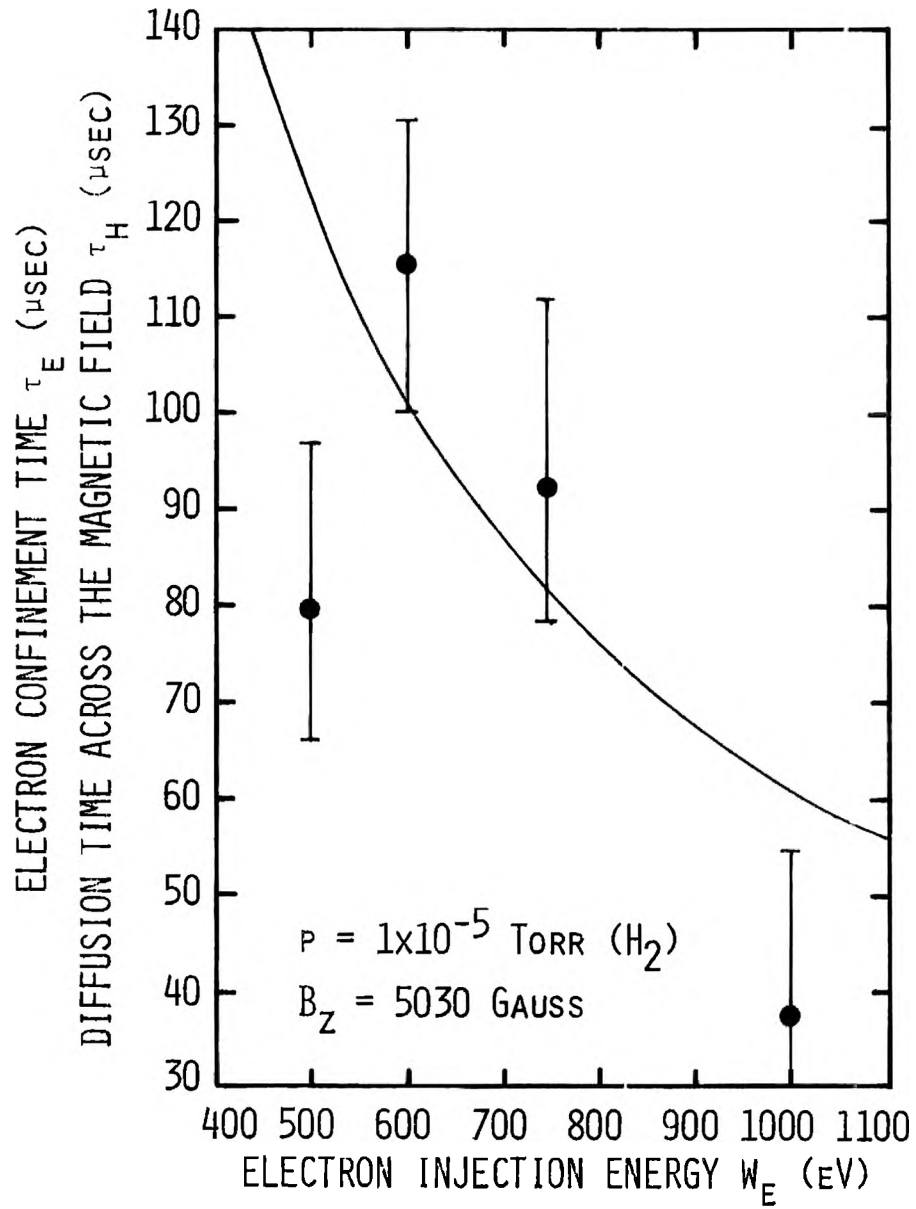Injection Energies of 600 and 750 eV.

Fig. 10. Dependence of Electron Confinement
Time on Injection Energy.

C. Electron Density

Figure 11 illustrates the electron density as a function of electron injection current at 500 eV injection energy and at a pressure of 10^{-5} Torr hydrogen gas for various magnetic fields in the point cusp. A voltage of -5000 volts was applied to the other point cusp and ring cusp cathodes. For each magnetic field, the electron density shows a rapid increase to about 2 mA injection current and changes to a gradual, almost linear, increase to 10 mA. If a linear least-square fit is drawn for the data to the right of I_e = 2 mA (Fig. 12), the electron density as a function of electron injection current and magnetic induction can be more easily seen.

From the linear portion of the B_z = 5030 Gauss curve in Fig. 11 or 12, the electron density is found to be approximately $(2.5 \pm 1.3) \times 10^{10}$ cm^{-3}.

The electron density in the central plasma region, calculated from Eq. (2-4), is approximately 1.5×10^{10} cm^{-3} for a magnetic induction of 5000 Gauss in the point cusp and an electron injection energy of 500 eV. The theoretical and experimental densities agree to within experimental error.

The dependence of electron density on injection current can be seen from the electron conservation equation[13]

$$\frac{dn_e}{dt} = \frac{I_e}{eV} + n_m \nu_m - \alpha_r n_e n_i - n_e \nu_H - n_e \nu_{ve}.$$

where ν_H and ν_{ve} are the electron diffusion loss rates across the magnetic field and in velocity space over the potential barrier Φ_e,
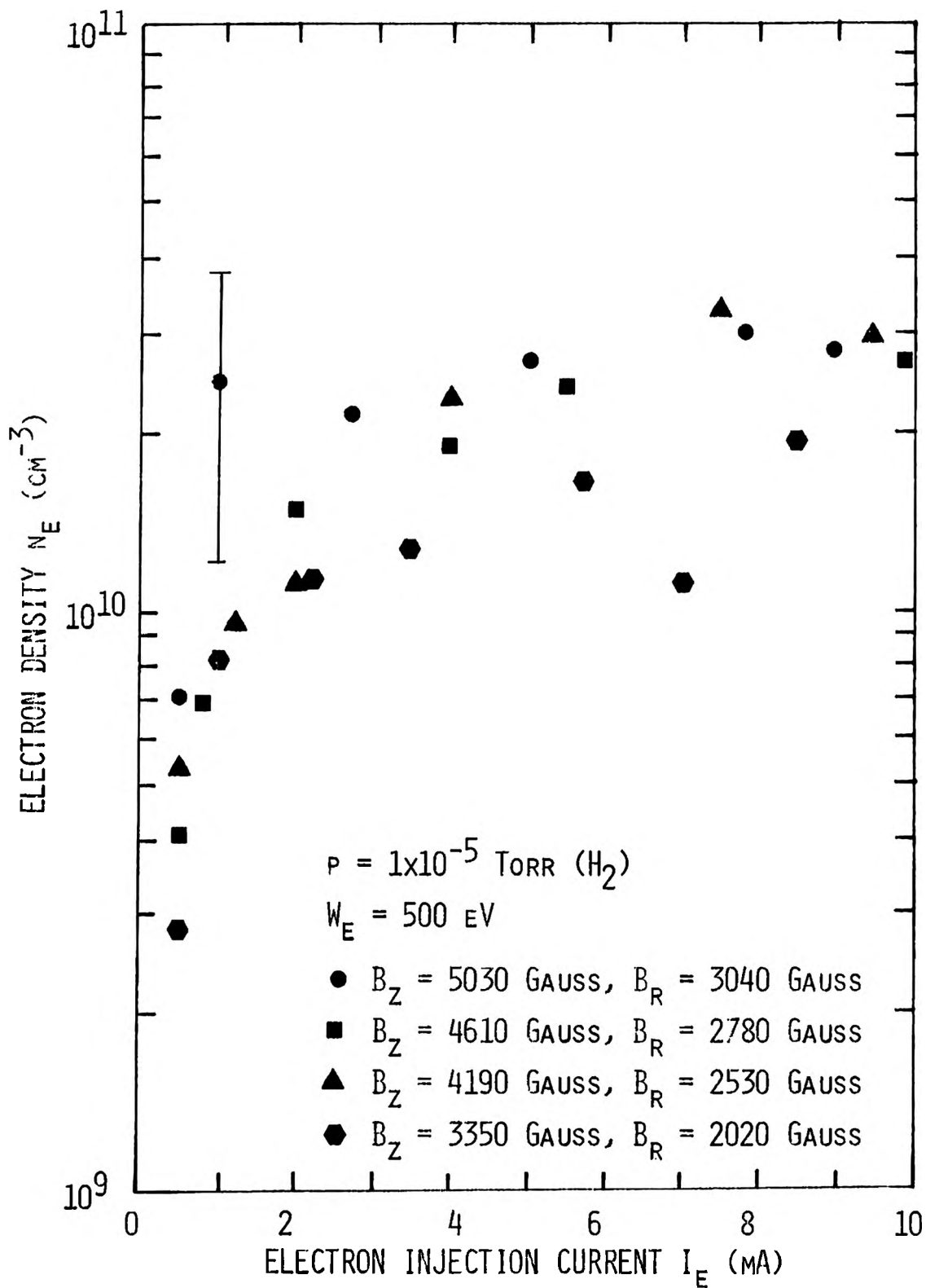
Fig. 11. Dependence of Electron Density on Injection
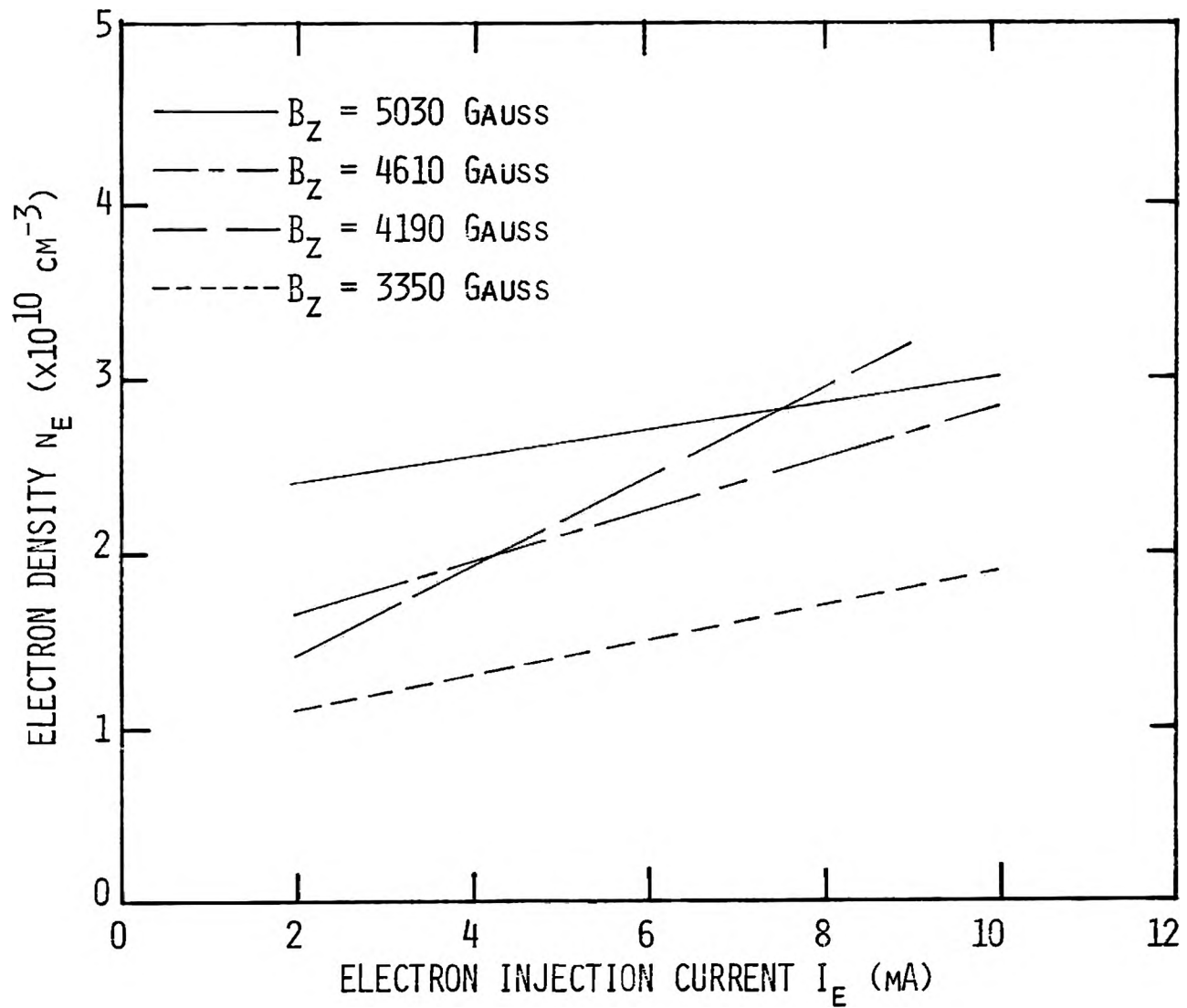Current for Different Magnetic Inductions.

Fig. 12. Dependence of Electron Density on Injection Current (Least-Squares Fit).

$n_m \nu_m$ is the effective plasma source due to ionization of incident

neutrals, n_i is the ion density, α_r is the effective recombination

coefficient and V is the plasma volume. The loss rates ν_H and ν_{ve}

are discussed in Ref. [12]. For the steady state condition, the

equation becomes

$$n_e = \frac{I_e/eV + n_m \nu_m}{(\nu_H + \nu_{ve} + \alpha_r n_i)} .$$
(4-2)

Initially, the electron density will increase as the injection

current is increased. This increase in density occurs because the

additional electrons will replace the electrons lost from the system,

increase the potential well depth and ionize neutral atoms. As the

injection current is increased further, the space charge limitations

in the anode cause $\Delta\Phi$ to become large and Φ_e to decrease, increasing

ν_{ve}. Any additional injection current will be lost through the cusp

openings. Thus, the electron density will reach some saturation

value and any further increase in the injection current will have no

effect on the density. The electron density associated with the

increasing $\Delta\Phi$ can be determined from Eqs. (2-2) and (2-4).

Figure 13 illustrates the results of injecting 500 eV electrons

into the magnetic trap at 10^{-5} Torr hydrogen gas and 4×10^{-6} Torr air

with B_z = 4190 Gauss. The electron density at the pressure of 4×10^{-6}

Torr air shows the same general behavior as at 10^{-5} Torr hydrogen.

The observed densities differ very little as a function of pressure.

However, the percentage of neutral gas ionized increases with

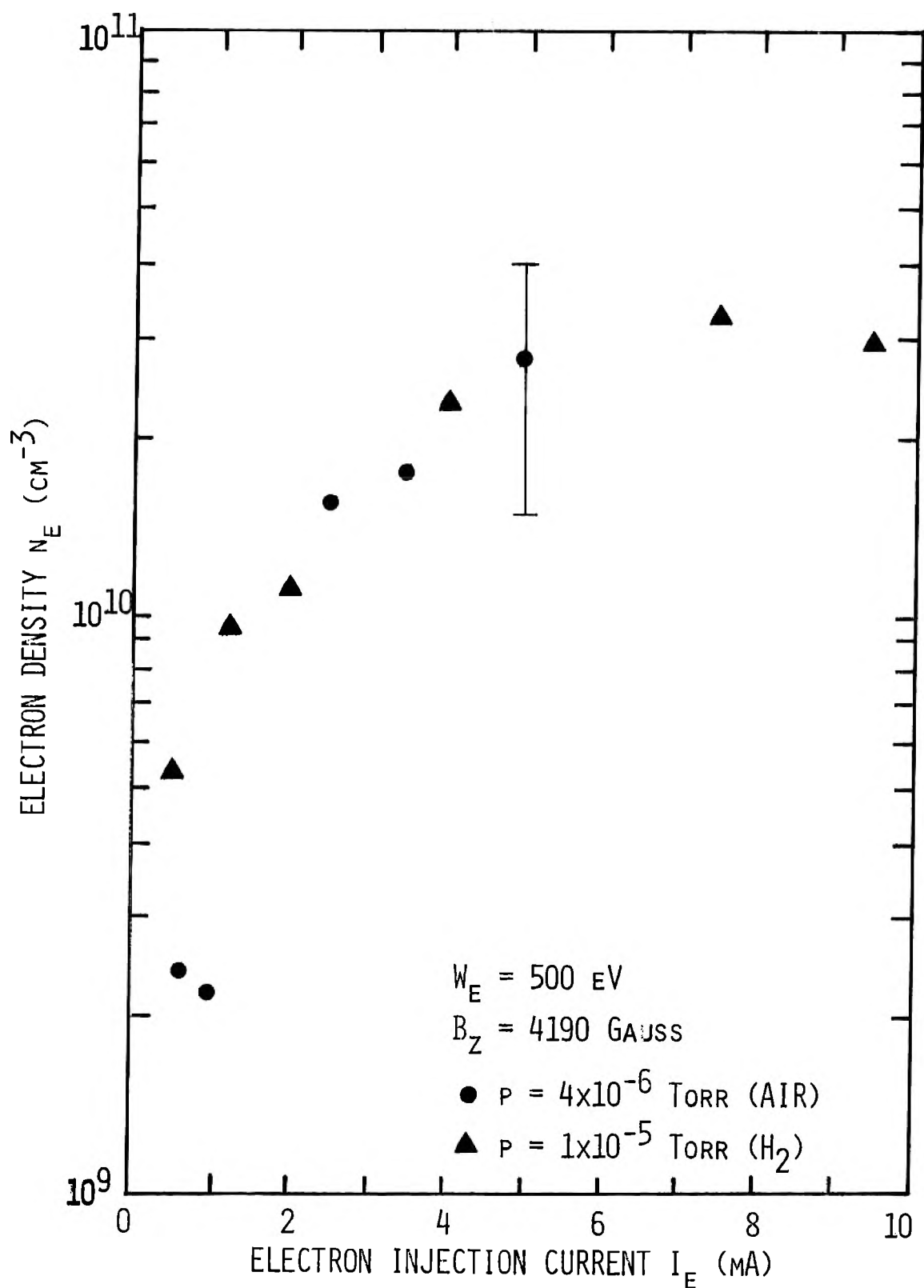decreasing pressure from about 6% at 10^{-5} Torr to about 14% at

Fig. 13. Dependence of Electron Density on Injection
Current for Different Pressures.

4×10^{-6} Torr.

The dependence of electron density on pressure can be seen through the expression for τ_H, Eq. (4-1), and the electron conservation equation, Eq. (4-2), where $\nu_H = \tau_H^{-1}$. The term $n_m \nu_m$ in Eq. (4-2) also depends on pressure where n_m is the density of the neutral atoms.

Figure 14 shows the electron density as a function of electron injection current for injection energies of 500 and 1000 eV at a pressure of 10^{-5} Torr hydrogen gas and a magnetic induction in the point cusp of 5030 Gauss. As shown, the electron density shows little dependence on injection energy. On the other hand, the data obtained by Pankrat'ev[21] using a different diagnostic technique showed the ion density increasing over two orders of magnitude for injection energies varying from 500 to 1500 eV. A simultaneous solution to a complete set of equations may provide better insight to the dependence of density on injection energy, but such theoretical studies are not yet complete.

Figure 15 shows a plot of the electron density from Figs. 11 or 12 versus the square of the magnetic induction for a constant injection current. The electron density appears to vary linearly with the square of the magnetic induction, however, the error bars are too large to permit firm conclusions.

If Eq. (2-3) for the Larmor radius in the point anode is substituted into Eq. (2-2), an equation showing explicitly the behavior of the electron density on the applied anode-to-cathode voltage and the magnetic induction is obtained. This equation is
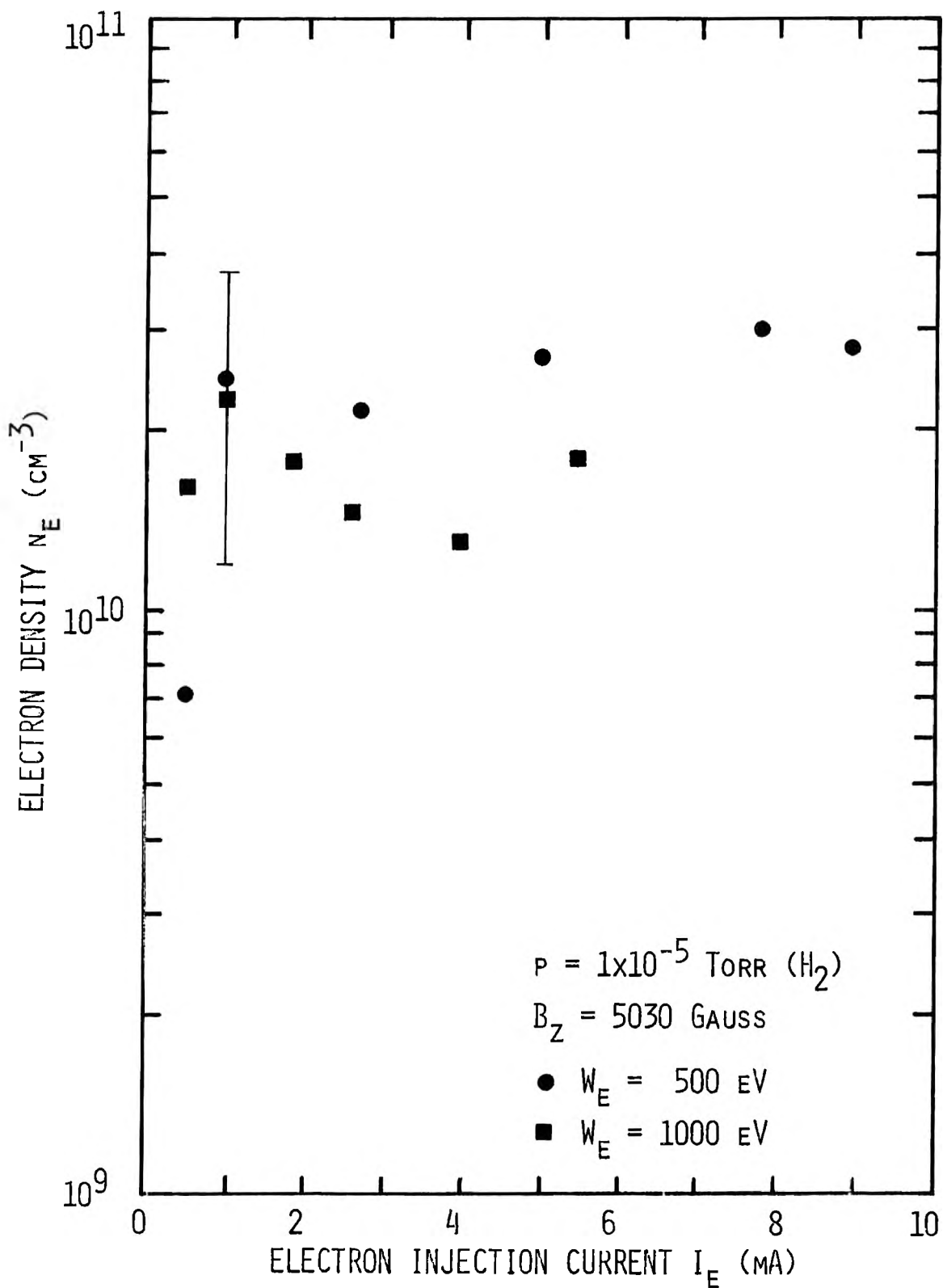
Fig. 14. Dependence of Electron Density on Injection
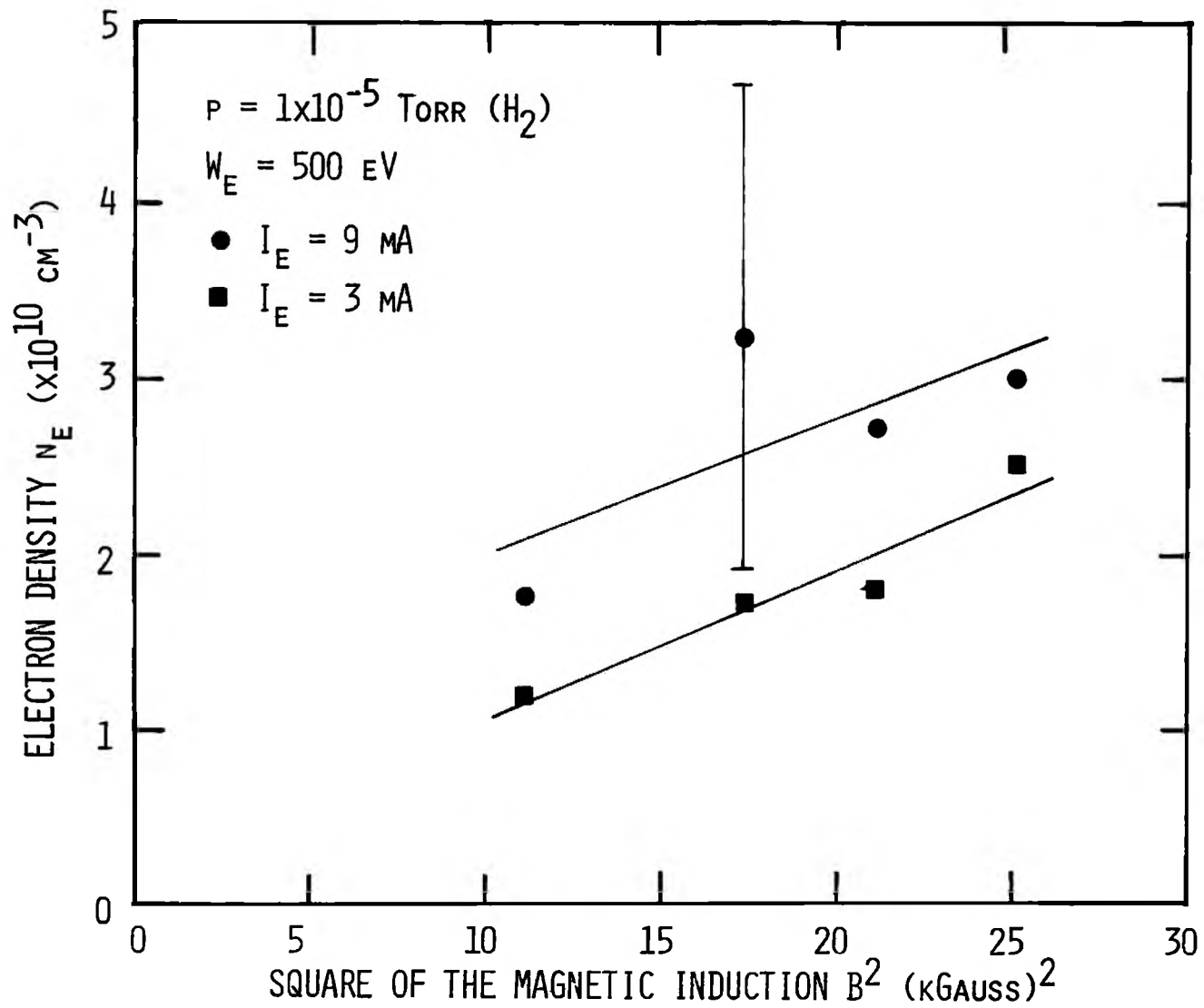Current for Different Injection Energies.

Fig. 15. Dependence of Electron Density on Magnetic Induction.

$$(n_A)_{point} = \frac{5.84 \times 10^7 \, f_1 \Phi_A B_z^2}{f_2^2 f_3 W_e [\frac{5}{9} + \frac{2}{3} \ln(\frac{a_p B_z}{3.37 f_2 (f_3 W_e)^{1/2}})]} \qquad (4\text{-}3)$$

where $f_1 = \Delta\Phi/\Phi_A$, $f_2 = r_1/r_{Lp}$ and $f_3 = \overline{W}_{e\perp}/W_e$. The injection energy is equal to $e\Phi_A$ because the injection voltage applied to the electron gun cathode is also the applied voltage. Using the parameters listed in Table I, it is found that $f_1 = 0.5$, $f_2 = 20$ and $f_3 = 0.55$. From Eq. (4-3), the electron density in the point anode and in the central plasma region will increase slightly with injection energy (or applied voltage) and with the square on the magnetic induction which is in general agreement with the results obtained from Figs. 14 and 15.

Summarizing, it is found that:

1. The error bars are quite large, typically about $\pm 1.3 \times 10^{10}$ cm^{-3}.

2. The electron density in the central plasma region is approximately 2.5×10^{10} cm^{-3}, Fig. 11 or 12, and agrees with the theoretical density to within experimental error for a $B_z = 5000$ Gauss, $W_e = 500$ eV and $p = 10^{-5}$ Torr.

3. The electron confinement time is 80 μsec, Fig. 10. Generally, the theoretical curve agrees with the experimental points to within an error of 65%.

4. The electron density rises very rapidly to about 2 mA injection current and then levels off to a gradual increase. The electron density also increases with magnetic field, Figs. 11 and 12. The theoretical dependence of electron density on injection current

is found in Eq. (4-2).

5. The electron density shows little dependence on pressure, Fig. 13, but the fraction of neutral gas ionized increases with decreasing pressure.

6. The electron density shows little dependence on injection energy, Fig. 14, but tends to vary linearly with the square of the magnetic induction, Fig. 15. The theoretical dependence on injection energy and magnetic induction indicates a behavior similar to Figs. 14 and 15.

V. CONCLUSIONS

The results indicate that the confinement scheme will confine a plasma and that the plasma behaves approximately as expected. The density generally increases with electron injection current and with magnetic induction. The plasma electron density, so far, is less than the neutral gas density. The theoretical estimate of electron density is consistent with experimental values for the UMR experiment. The theoretical and experimental electron confinement times agree to within 65%.

If the modifications (see Appendix E) increase the electron density as planned, more meaningful data can be obtained and a complete parametric study over a full range of electron injection energies, pressure and magnetic induction should be possible.

BIBLIOGRAPHY

[1]   Lavrent'ev, O. A., "Electrostatic and Electromagnetic High
      Temperature Plasma Traps," Electromagnetic Plasma
      Confinement and the Phenomenology of Relativistic
      Electron Beams, Ann. N. Y. Acad. Sci., Vol. 251,
      New York, 152, 1975.

[2]   Pankrat'ev, Yu. I., et al., "Accumulation of Plasma by
      Ionization of a Residual Gas in an Electromagnetic
      Trap," Atomnaya Energiya 32, No. 1, 131(1972).

[3]   Pankrat'ev, Yu. I., et al., "Plasma Losses in the Ring Gap
      of an Electromagnetic Trap," Atomnaya Energiya 35,
      No. 4, 253(1973).

[4]   Stansfield, B. L., Larsen, J. M., et al., "Progress Report on
      the KEMP II Experiment: Plasma Confinement in an
      Electrostatically Stoppered Spindle Cusp Magnetic Field,"
      Electromagnetic Plasma Confinement and the Phenomenology
      of Relativistic Electron Beams, Ann. N. Y. Acad. Sci.,
      Vol. 251, New York, 367, 1975.

[5]   Ware, A. A., and Faulkner, J. E., "Electrostatic Plugging of
      Open-Ended Magnetic Containment Systems," Nuclear Fusion
      9, 353(1969).

[6]   Moir, R. W., Barr, W. L., and Post, R. F., "Experimental
      Results on Electrostatic Stoppering," Phys. Fluids 14,
      No. 11, 2531(1971).

[7]   Osher, J. E., Foreign Trip Report: U.S.S.R. Exploratory
      Exchange, Lawrence Livermore Laboratory, (Dec. 1974).

[8]   Perkins, W. A., and Brown, J. C., "MAFCO-A Magnetic Field
      Code for Handling General Current Elements in Three
      Dimensions," Report UCRL-7744-Rev. II. Lawrence
      Livermore Laboratory (1966).

[9]   Operating Manual, Model 715A Klystron Power Supply,
      Hewlett-Packard Co., Palo Alto, California, 1956.

[10] "Reflex Klystron Operation and Microwave Power and Frequency
      Measurements," EE 230 Lab, Experiment #3, University of
      Missouri-Rolla, 1974. (unpublished)

[11] Lance, A. L., Introduction to Microwave Theory and
      Measurements, McGraw-Hill, Inc., New York, 1964.

BIBLIOGRAPHY (cont.)

[12] Dolan, T. J., Larsen, J. M., and Stansfield, B. L.,
      "Theoretical Confinement Times in Electromagnetic Traps,"
      to be published in Can. J. Phys.

[13] Dolan, T. J., Stansfield, B. L., and Larsen, J. M., "Plasma
      Potential in Electrostatically-Plugged Cusps and
      Mirrors," to be published in Phys. Fluids.

[14] Bernstein, I. B., and Terhan, S. K., "Plasma Oscillations (1),"
      Nuclear Fusion 1, 3(1960).

[15] Heald, M. A., and Wharton, C. B., Plasma Diagnostics With
      Microwaves, John Wiley and Sons, Inc., New York, 1965.

[16] Krall, N. A., and Trivelpiece, A. W., Principles of Plasma
      Physics, McGraw-Hill, Inc., New York, 1973.

[17] Seshadri, S. R., Fundamentals of Plasma Physics, American
      Elsevier Publ. Co., Inc., New York, 1973.

[18] Chen, F. F., Introduction to Plasma Physics, Plenum Press,
      New York, 1974.

VITA

Robert L. Hayward was born on May 25, 1946, in Newport News, Virginia. He was raised in Mineola, Iowa and graduated from Glenwood Community High School, Glenwood, Iowa, in May 1964. He attended Northwest Missouri State University where he married the former Nona Langford. In August, 1968, he received his B.S. in Physics and Mathematics from NWMSU. He taught physics and science at Buchanan High School in Troy, Missouri the following year. After teaching school for one year, he enlisted in the U.S. Air Force.

The author has been enrolled in graduate school in the Nuclear Engineering Department at the University of Missouri-Rolla since August, 1973.

The author is a member of Phi Kappa Phi National Honor Society and the American Nuclear Society.

APPENDIX A

OPERATION OF THE PLASMA CONFINEMENT DEVICE

There are four precautions that must be taken while operating the experiment. Two of these are related to potential health hazards.

1. Avoid electrical shock.

2. Avoid eye hazards (from glass breaking on vacuum system).

The other two involve potential damage to the equipment.

3. The cooling water to the magnet coils must be flowing under 40 psi pressure before and while the welders are operating.

4. The klystron cooling fan must blow a stream of air across the klystron while its power supply is operating.

The procedure for operating the cusp device is as follows:

1. Turn on the klystron cooling fan.

2. Turn on the main power switch to the klystron power supply and turn the modulation switch to CW to allow the klystron and power supply to warm up.

3. Turn on the cooling water pump. The pressure should indicate 40 psi pressure.

4. Check the magnet cables and high voltage cables to the ring and point cusp cathodes for possible shorts.

5. Turn on the power supply to the electron gun filament and gradually increase the current through the filament.

6. Perform the power peaking and alignment procedure as described earlier.

7. Turn on the ring and point cusp power supplies and set for the desired voltages.

8. Energize the magnetic field and set for the desired current.

9. Turn on the power supply for the electron gun injection

    voltage and set for the desired voltage.

10. Perform the experiment.

Figure 16 is a checklist for recording initial settings. Close

attention should be kept to the magnet coil outlet water temperature.

The temperature in the two hottest hoses should not exceed 85°C.

For shutdown, all power supplies should be turned off. The

klystron cooling fan should remain on for a few minutes after

shutdown to provide additional cooling of the klystron. The power

supply to the electron gun filament should be turned down until

the filament glows dimly.

ELECTROMAGNETIC CUSP EXPERIMENT: EQUIPMENT CHECKLIST AND SETTINGS

operator & assistant . . . . ._____

date/starting time . . . . ._____

cooling water pressure . . . . . . (psi) ._____

check magnet cables. . . . . ._____

east welder, voltage . . . . (V) . ._____

           current . . . . (A) . ._____

west welder, voltage . . . . (V) . ._____

           current . . . . (A) . ._____

water temperature. . . . . ._____

           inlet . . . . (C) . ._____

           outlet. . . . . (C) . ._____

point cusp voltage . . . . (kV). ._____

ring cusp voltage. . . . . (kV). ._____

cathode heater . . . . ._____

           variac. . . . . (div) ._____

           voltage . . . . (V) . ._____

           current . . . . (A) . ._____

klystron fan on? . . . . ._____

           beam voltage. . . . . (V) . ._____

           reflector voltage . . (V) . ._____

           current . . . . (mA). ._____

initial pressure, log scale. . . . (Torr)._____

pulser parameters, if used . . . . ._____

Fig. 16.   Electromagnetic Cusp Experiment:
Equipment Checklist and Settings.

APPENDIX B

PROBLEMS ENCOUNTERED IN OPERATING THE EXPERIMENT

Several problems have been encountered which should be mentioned. The present electron gun filament design, as mentioned earlier, is two layers of thoriated tungsten mesh approximately 0.6 cm^2 in area. Several other filament designs have been tried, none of which has worked satisfactorily. Some of these designs are: directly and indirectly heated tantalum wire and foil with and without a lanthanum hexaboride coating, tungsten mesh with coatings of strontium-barium-calcium oxide, and lanthanum hexaboride. The filaments have either overheated (with the coating sputtered onto the ceramic insulators), or the coatings became too brittle and broke off, or the wire mesh overheated and tore in half.

Another problem encountered was the inability of the ring cathode to hold a large voltage. Upon taking the chamber apart at the main flange, a small screw which had fallen down into the ring gap region was found. It had shorted the cathode to the chamber wall. Later, it was found that the screw probably came from a microwave antenna flange.

During the time the chamber was disassembled, a flat steel ring was installed on each of the ring anode surfaces with eight screws. The purpose of the ring was to reduce the anode gap thickness from 0.76 cm to 0.3 cm for the reasons stated in section II-B. A few months later there was trouble obtaining a plasma. After several attempts to correct the problem, the chamber was disassembled. One of the anode rings had warped and melted in two different places. The warped ring had partially blocked the anode gap and shorted the plasma electron sheath to ground.

One problem which has been bothersome from the beginning is a poor base pressure in the chamber (10^{-6} Torr). Whenever heat was applied to a diagnostic port containing a microwave waveguide and antenna for the purpose of baking out the chamber, the pressure would rise to a very high level. Upon disassembling the chamber for modifications, it was found that this port, when cleaned with acid, apparently had not been thoroughly rinsed with water and some green powder had formed on the waveguide and inside the port.

APPENDIX C

DERIVATION OF A GENERAL DISPERSION RELATION FOR AN

ELECTROMAGNETIC WAVE PROPAGATING THROUGH A PLASMA

There are two levels of approach to plasma theory. The first

of these is based on the direct solution of the Boltzmann transport

equation. This approach is also referred to as the microscopic,

statistical or kinetic theory description. The kinetic theory

approach is capable of providing a more complete description of the

dynamics of the plasma. However, this procedure is mathematically

more difficult. The second method is based on using a closed set

of moment equations derived from the Boltzmann equation to describe

the behavior of the plasma. This description (also referred to as

the macroscopic, hydrodynamic or fluid description) describes the

plasma in such quantities as number density, average velocity,

pressure and temperature. This method has the merit of relative

mathematical simplicity and is applicable when the phase velocity (v_p

$=\omega/k$) of the wave is much greater than the characteristic thermal

speed in a collision-free plasma (referred to as the "low

temperature approximation")[14].

The moment equations and Maxwell's equations will be used to

obtain the desired dispersion relation. The dispersion relation as

derived from the kinetic theory is given in Ref. [15] p. 111. For

plasma parameters expected for the UMR experiment, this relation will

reduce to the same relation as derived from the fluid equations.

A plasma consists of a collection of electrons and positive ions

with each species described by a distribution function $f(\vec{r},\vec{v},t)$ such

that $f(\vec{r},\vec{v},t)\ d\vec{r}\ d\vec{v}$ represents at time t the probable number of

particles with velocities between $\vec{v}$ and $\vec{v} + d\vec{v}$ and with positions

between $\vec{r}$ and $\vec{r} + d\vec{r}$. Some of the macroscopic variables are defined

as [16]:

a) The number of particles at position $\vec{r}$ at time t is given by

$$n(\vec{r},t) = \bar{n}\int f(\vec{r},\vec{v},t) \ d\vec{v}$$

where $\bar{n}$ is the total number of particles of a given species divided by the volume of the plasma.

b) The average velocity of the particles at position $\vec{r}$ and time t is given by

$$\vec{V}(\vec{r},t) = \frac{\int \vec{v}f(\vec{r},\vec{v},t) \ d\vec{v}}{\int f(\vec{r},\vec{v},t) \ d\vec{v}}$$

c) Similarly, the current density is given by

$$\vec{J}(\vec{r},t) = \sum_{\alpha} q_{\alpha}n_{\alpha}\int \vec{v}f(\vec{r},\vec{v},t) \ d\vec{v}$$

$$= \sum_{\alpha} q_{\alpha}n_{\alpha}(\vec{r},t)\vec{V}_{\alpha}(\vec{r},t)$$

where the summation is over the various particle species α and q_{α} is the electronic charge of the species under consideration,

d) and the pressure tensor,

$$\vec{P}(\vec{r},t) = \bar{n} \ m\int (\vec{v} - \vec{V})(\vec{v} - \vec{V})f(\vec{r},\vec{v},t) \ dv.$$

The Boltzmann transport equation is

$$(\frac{\partial}{\partial t} + \vec{v}\cdot\nabla_{r} + \vec{a}\cdot\nabla_{v})f(\vec{r},\vec{v},t) = (\frac{\partial f}{\partial t})_{collisions} \qquad (C-1)$$

where ∇_{r} and ∇_{v} represent the gradient operators in coordinate, $\vec{r}$, and

velocity, $\vec{v}$, space respectively. $(\frac{\partial f}{\partial t})_{coll}$ represents the time rate of change of f resulting from collisions. $\vec{v}$ and $\vec{a}$ ($\equiv \vec{F}/m$) represents the velocity and acceleration of the individual particles. There is a separate Boltzmann equation for each particle species. $\vec{F}$ can be adequately represented by the Lorentz force

$$\vec{F} = q\,\vec{E}(r,t) + q\,\frac{\vec{v}\times\vec{B}(\vec{r},t)}{c}$$

where $\vec{E}$ and $\vec{B}$ denote the electric and magnetic fields respectively which satisfy Maxwell's equations

$$\nabla\times\vec{B} = \frac{4\pi}{c}\,\vec{J} + \frac{1}{c}\frac{\partial\vec{E}}{\partial t} \tag{C-2}$$

$$\nabla\times\vec{E} = -\frac{1}{c}\frac{\partial\vec{B}}{\partial t} \tag{C-3}$$

$$\nabla\cdot\vec{E} = 4\pi\rho_q \text{ and } \nabla\cdot\vec{B} = 0 \tag{C-4}$$

where $\rho_q = \sum\limits_{\alpha} n_\alpha q_\alpha$.

Multiplying Eq. (C-1) by 1, $m\vec{v}$, and $m\vec{v}\vec{v}$, and assuming f becomes sufficiently small at large values of the velocity, the following moment equations for each particle species are obtained[14,16,17],

$$\frac{\partial n}{\partial t} + \nabla\cdot n\vec{V} = 0 \tag{C-5}$$

$$nm(\frac{\partial}{\partial t} + \vec{V}\cdot\nabla)\vec{V} - nq(\vec{E} + \frac{\vec{V}\times\vec{B}}{c}) + \nabla\cdot\vec{P} = -m\int n v(\frac{\partial f}{\partial t})_{coll}\,dv \tag{C-6}$$

$$\frac{\partial}{\partial t} \vec{P} + \nabla \cdot (\vec{Q} + \vec{V}_0 \vec{P}) + \vec{P} \cdot \nabla \vec{V}_0 + (\vec{P} \cdot \nabla \vec{V}_0)^T + \frac{q}{mc}(\vec{B} \times \vec{P} - \vec{P} \times \vec{B})$$

$$- mn[\frac{q}{m}(\vec{E} + \frac{1}{c}\vec{V}_0 \times \vec{B})]\vec{V} - mn\vec{V}[\frac{q}{m}(\vec{E} + \frac{1}{c}\vec{V}_0 \times \vec{B})] + mn[\frac{d}{dt}\vec{V}_0\vec{V} + \vec{V}\frac{d}{dt}\vec{V}_0]$$

$$= (\frac{\partial}{\partial t}\vec{P}_{coll}) \qquad\qquad (C-7)$$

where A^T denotes the transpose of A and $\vec{V}_0$ is the velocity of the center of mass of the particles. Summing these equations over all species of the system and assuming only electrons and one species of ions, the following equations are obtained[14,16,17],

$$\frac{\partial}{\partial t}\rho_q + \nabla \cdot \vec{J} = 0,$$

$$\rho_m \frac{\partial}{\partial t}\vec{V} + \rho_m(\vec{V} \cdot \nabla)\vec{V} - \rho_q\vec{E} - \frac{\vec{J} \times \vec{B}}{c} + \nabla \cdot \vec{P} = 0,$$

$$\frac{\partial}{\partial t}\vec{P} + \nabla \cdot (\vec{Q} + \vec{V}\vec{P}) + \vec{P} \cdot \nabla\vec{V} + (\vec{P} \cdot \nabla\vec{V})^T + \frac{e}{mc}(\vec{B} \times \vec{P} - \vec{P} \times \vec{B})$$

$$- (\vec{J} - \rho_q\vec{V})(\vec{E} + \frac{1}{c}\vec{V} \times \vec{B}) - (\vec{E} + \frac{1}{c}\vec{V} \times \vec{B})(\vec{J} - \rho_q\vec{V}) = \frac{\partial}{\partial t}\vec{P}$$

where ρ_q and ρ_m are the charge and mass densities, e is the electronic charge (esu), $\vec{Q}$ is the heat flow tensor and $\vec{J}$ is the total current density. These equations are respectively referred to as the equation of continuity, equation of momentum transfer and the equation of motion of the pressure tensor. An equation for $\vec{Q}$ could be obtained by taking the third moment of the Boltzmann equation, however, this equation would involve higher moments of the distribution function and again the system of equations would not be

closed. The system of equations can be terminated by setting $\nabla \cdot \vec{Q} = 0$ which is equivalent to assuming there is no heat flow in the system (see Ref. [17] p. 46).

In studying wave phenomena, high frequency oscillations will perturb the electrons and have a lesser effect on the positive ions, creating regions of local charge density ρ_q. Thus, as an approximation, only the equations for electrons will be used.

Consider a uniform plasma of electron density n_0 at rest in a uniform magnetic field, $\vec{B}_0$, with no electric field or plasma currents present. Assume that a plane electromagnetic wave is traveling in the direction of the vector wave number $\vec{k}$ and perturbs the plasma such that

$$n = n_0 + n_1 \qquad n_1 \ll n_0$$

$$\vec{V} = \vec{V}_1$$

$$\vec{J} = \vec{J}_1$$

$$\vec{E} = \vec{E}_1$$

$$\vec{B} = \vec{B}_0 + \vec{B}_1 \qquad \vec{B}_1 \ll \vec{B}_0$$

$$\vec{P} = p\vec{I} + \vec{P}_1 \qquad \text{(C-8)}$$

where the zero subscript terms refer to the constant equilibrium quantities and the one subscript terms refer to the space and time perturbed quantities. $\vec{I}$ is the identity matrix. $p(= n\kappa T)$ is the equilibrium scalar pressure. $\vec{P}_1$ allows for anisotropy of the pressure tensor during perturbation[14]. Substitute Eq. (C-8) into the fluid

equations, Eqs. (C-5) to (C-7), for electrons to obtain a set of linearized moment equations

$$\frac{\partial}{\partial t} n_1 - \frac{1}{e} \nabla \cdot \vec{J}_1 = 0 \qquad\qquad (C-9)$$

$$- \frac{m}{e} \frac{\partial}{\partial t} \vec{J}_1 + n_0 e \vec{E}_1 - \frac{1}{c} \vec{J}_1 \times \vec{B}_0 + \nabla \cdot \vec{P}_1 = 0 \qquad\qquad (C-10)$$

$$\frac{\partial}{\partial t} \vec{P}_1 - \frac{\kappa T}{e} [\nabla \cdot \vec{J}_1 \vec{I} + \nabla \vec{J}_1 + (\nabla \vec{J}_1)^T] = 0 \qquad\qquad (C-11)$$

where collisions, all second order terms in the equation of continuity and in the equation for momentum transfer, all nonlinear terms, and those involving the magnetic field in the equation of motion of the pressure tensor have been neglected. These are essentially the assumptions of low temperature and weak magnetic fields[14,15].

Assume the perturbed electric field and current density vary in space and time as

$$\vec{E}_1 = \tilde{E}_1 e^{i(\vec{k} \cdot \vec{r} - \omega t)}$$

$$\vec{J}_1 = \tilde{J}_1 e^{i(\vec{k} \cdot \vec{r} - \omega t)}. \qquad\qquad (C-12)$$

Taking the divergence of Eq. (C-11) to obtain

$$\frac{\partial}{\partial t} (\nabla \cdot \vec{P}_1) - \frac{\kappa T}{e} [2\nabla (\nabla \cdot \vec{J}_1) + (\nabla \cdot \nabla) \vec{J}_1] = 0. \qquad\qquad (C-13)$$

Solve Eq. (C-10) for $\nabla \cdot \vec{P}_1$, substitute this into Eq. (C-13) and use Eq. (C-12) to obtain

$$i \frac{m\omega}{e} \tilde{J}_1 + n_0 e \tilde{E}_1 + \frac{\vec{B}_0 \times \vec{J}_1}{c} - \frac{T}{e}[2\vec{k}\vec{k}\cdot + \vec{k}\cdot\vec{k}]\tilde{J}_1 = 0.$$

Rearranging the equation to obtain

$$\tilde{E}_1 = -i \ 4\pi \left(\frac{\omega}{\omega_p^2}\right) [1 - i(\frac{\vec{\omega}_{ce}}{\omega} \times) - \frac{\kappa T}{m\omega^2}(2\vec{k}\vec{k}\cdot + \vec{k}\cdot\vec{k})]\tilde{J}_1 = 0 \qquad (C-14)$$

where

$$\omega_p = \left(\frac{4\pi n_e e^2}{m}\right)^{1/2} = 5.64\times10^4 (n_e)^{1/2} \frac{radians}{sec}$$

$$\vec{\omega}_{ce} = \frac{e\vec{B}_0}{mc} = 1.76\times10^7 B_0 [Gauss] \frac{radians}{sec}$$

are referred to as the plasma frequency and the electron cyclotron resonance frequency, respectively. The coefficient of $\tilde{J}_1$ is the tensor resistivity, σ^{-1}, of the plasma. It can be inverted to obtain the plasma conductivity tensor $\vec{\sigma}$ and dielectric tensor $\vec{\epsilon}$.

Without loss of generality, a coordinate system can be choosen where the z-axis lies along the steady magnetic field, $\vec{B}_0$, and the vector $\vec{k}$ lies in the x-z plane. Thus, $\vec{k}$ and $\vec{\omega}_{ce}$ can be written as

$$\vec{k} = \vec{\mu}(\omega/c)(\xi,0,\zeta)$$

$$\vec{\omega}_{ce} = (0,0,\omega_{ce})$$

where μ is the index of refraction (= c/v_p), v_p is the phase velocity, ξ and ζ are the direction cosines of $\vec{k}$. $\vec{k}$ and $\vec{\mu}$ can be complex. From equation (C-14), the coefficient of $\tilde{J}_1$ becomes, in matrix form

$$\sigma^{-1} = -i\ 4\pi\ \frac{\omega}{\omega_p^2} \begin{vmatrix} 1-\delta(1+2\xi^2) & i\gamma & -2\delta\xi\zeta \\ \\ -i\gamma & 1-\delta & 0 \\ \\ -2\delta\xi\zeta & 0 & 1-\delta(1+2\zeta^2) \end{vmatrix}$$

where

$$\gamma = \frac{\omega_{ce}}{\omega} \text{ and } \delta = \mu^2\ \frac{\kappa T}{mc^2}\ .$$

Note that δ is the square of the ratio of the electron thermal speed to wave phase velocity which is required to be small for the low temperature approximation. The reciprocal of the resistivity is the conductivity

$$\sigma = i \frac{\omega_p^2/(4\pi\omega)}{(1-\delta)^2(1-3\delta) - \gamma^2[1-\delta(1+2\zeta^2)]}$$

$$X \begin{vmatrix} 1-2\delta(1+\zeta^2) + \delta^2(1+2\zeta^2) & -i\gamma[1-\delta(1+2\zeta^2)] & 2\delta\xi\zeta(1-\delta) \\ \\ i\gamma[1-\delta(1+2\zeta^2)] & 1-4\delta+3\delta^2 & i2\gamma\delta\xi\zeta \\ \\ 2\delta\xi\zeta(1-\delta) & -i2\gamma\delta\xi\zeta & \begin{matrix}1-2\delta(1+\xi^2) \\ +\delta^2(1+2\xi^2) - \gamma^2\end{matrix} \end{vmatrix} \quad \text{(C-15)}$$

where the coefficient is understood to multiply each element of the matrix.

The linearized form of Maxwell's equations, Eqs. (C-3) and (C-4), are

$$\nabla\times\vec{B}_1 = \frac{4\pi}{c}\ \vec{J}_1 + \frac{1}{c}\ \frac{\partial}{\partial t}\ \vec{E}_1 \quad \text{(C-16)}$$

$$\nabla \times \vec{E}_1 = -\frac{1}{c}\frac{\partial}{\partial t}\vec{B}_1. \qquad (C-17)$$

Substitute Eq. (C-16) into the curl of Eq. (C-17) and use Eq. (C-12) to obtain

$$\vec{k}\times\vec{k}\times\tilde{E}_1 + \frac{\omega^2}{c^2}\vec{\epsilon}\cdot\vec{E}_1 = 0 \qquad (C-18)$$

where

$$\vec{\epsilon} = \vec{I} + i\frac{4\pi\vec{\sigma}}{\omega}. \qquad (C-19)$$

Eq. (C-18) can be written as

$$[\vec{k}\times\vec{k}\times + \frac{\omega^2}{c^2}\vec{\epsilon}\cdot]\tilde{E}_1 = 0. \qquad (C-20)$$

This is a set of homogeneous equations. The determinant of the coefficients of $\tilde{E}_1$ must vanish to insure a nontrivial solution. For $\vec{k}$ in the x-z plane and using Eqs. (C-15) and (C-19), this condition becomes

$$\begin{vmatrix} 1-\mu^2\zeta^2-\sigma_{xx} & -\sigma_{xy} & \mu^2\xi\zeta-\sigma_{xz} \\ \\ -\sigma_{yx} & 1-\mu^2-\sigma_{yy} & -\sigma_{yz} \\ \\ \mu^2\xi\zeta-\sigma_{zx} & -\sigma_{zy} & 1-\mu^2\xi^2-\sigma_{zz} \end{vmatrix} = 0 \qquad (C-21)$$

where σ_{xx}, σ_{xy}, $\cdots$ are the respective elements of the conductivity tensor each multiplied by

$$\frac{(\omega_p/\omega)^2}{(1-\delta)^2(1-3\delta) - Y^2[1-\delta(1+2\zeta^2)]} \;. \tag{C-21a}$$

If $\xi=1$ and $\zeta=0$ in Eqs. (C-21) and (C-21a), the dispersion relation

for wave propagation perpendicular to the external magnetic field,

$\vec{B}_0$ is obtained. This dispersion relation has two components, one

component for $\vec{E}$ of the wave parallel to $\vec{B}_0$ ("ordinary wave") and the

other component for $\vec{E}$ of the wave perpendicular to $\vec{B}_0$ ("extraordinary

wave"). The dispersion relation for wave propagation parallel to the

external magnetic field is obtained by setting $\xi=0$ and $\zeta=1$ in

Eqs. (C-21) and (C-21a). There are three components to this

dispersion relation, a left and a right circularly polarized wave

and wave motion parallel to the external magnetic field. See

Ref. [16], pp. 182-200 and Ref. [18], chapter 4, for additional

discussion of the different waves. Propagation at any angle other

than the two mentioned is possible but the dispersion relation

becomes quite complicated.

For propagation perpendicular to the external magnetic field,

Eqs. (C-21) and (C-21a) combine to give

$$[\mu^2 - 1 + \frac{(\omega_p/\omega)^2}{(1-\delta)}]\{[1 - \frac{(\omega_p/\omega)^2(1-\delta)}{[(1-\delta)(1-3\delta)-(\omega_{ce}/\omega)^2]}]\mu^2$$

$$- [1 - (\frac{\omega_p}{\omega})^2 \frac{2 - (\omega_p/\omega)^2 - 4\delta}{[(1-\delta)(1-3\delta)-(\omega_{ce}/\omega)^2]}]\} = 0. \tag{C-22}$$

In the approximation of low temperature, the ordinary wave is

not coupled to the magnetic field and the expression in the first bracketed term is used. The second bracketed term represents the dispersion relation for the "extraordinary wave", with $\vec{E}$ polarized perpendicular to $\vec{B}_0$. This term is coupled to the magnetic field through the expression for ω_{ce}. To first order in temperature

$$\mu^2_{ord} = 1 - \frac{(\omega_p/\omega)^2}{1 - \frac{\kappa T}{mc^2}[1 - (\frac{\omega_p}{\omega})^2]}$$

or

$$k^2_p \simeq \frac{\omega^2}{c^2}[1 - (\frac{\omega_p}{\omega})^2][1 - (\frac{\omega_p}{\omega})^2 \frac{\kappa T}{mc^2}] \tag{C-23}$$

where k_p is the wave number for the ordinary electromagnetic wave propagating through the plasma. For the expected range of electron temperatures and densities (see Table I) Eq. (C-23) reduces to

$$k^2_p \simeq \frac{\omega^2}{c^2}[1 - (\frac{\omega_p}{\omega})^2]. \tag{C-24}$$

This is the dispersion relation to be used in relating the electron density to microwave data.

APPENDIX D

EFFECTS OF OTHER WAVE MODES

Equation (3-4) gives the dispersion relation for an electromagnetic wave with its $\vec{E}$ vector parallel to $\vec{B}_0$ and propagating perpendicular to $\vec{B}_0$. However, since the direction of the magnetic field is changing along the propagation path of the electromagnetic wave, both $\vec{k}_p$ and its $\vec{E}$ vector will have components parallel and perpendicular to $\vec{B}_0$. $\vec{k}_p$ can be considered as the resultant of several waves propagating through the plasma. There are four waves of interest. These are (see Ref. [18] p. 130):

ordinary wave: $\vec{k} \perp \vec{B}_0$, $\vec{E} \parallel \vec{B}_0$

$$k_{ord} = (\omega/c)^2 [1 - (\omega_p/\omega)^2]$$ (D-1)

extraordinary wave: $\vec{k} \perp \vec{B}_0$, $\vec{E} \perp \vec{B}_0$

$$k_{ex} = (\omega/c)^2 [1 - \{\frac{1 - (\omega_p/\omega)^2}{1 - (\frac{\omega_{ce}^2 + \omega_p^2}{\omega^2})}\}]$$ (D-2)

left and right hand circularly polarized wave: $\vec{k} \parallel \vec{B}_0$, $\vec{E} \perp \vec{B}_0$

$$k_{l,r} = (\omega/c)^2 [1 - \frac{(\omega_p/\omega)^2}{1 \pm \omega_{ce}/\omega}]$$ (D-3)

where the temperature correction term, $[1 - (\omega_p/\omega)^2 \kappa T/mc^2]$, has been neglected since this term is approximately equal to one for this experiment.

The wave propagation vector through the plasma can be represented as

$$k_p^2 = xk_{ord}^2 + yk_{ex}^2 + (1-x-y)k_{1,r}^2 \qquad \text{(D-4)}$$

where x and y are the fractions of the total wave comprising the ordinary and the extraordinary wave, respectively, and (1-x-y) is the fraction with $\vec{k}_p$ parallel to $\vec{B}_0$. The values of these fractions are determined mainly by the angle between $\vec{k}_p$ and $\vec{B}_0$. This angle varies along the propagation path and with the distance from the center line connecting the two waveguide antennas.

Substitute Eqs. (D-1), (D-2) and (D-3) into Eq. (D-4) and expand the denominator in the last two terms to obtain

$$k_p = (1+z)^{1/2} k_{ord} \qquad \text{(D-5)}$$

where

$$z = \frac{y[-b^2(1-b^2)(1+c^2+c^4+\cdots)+b^2]}{(1-b^2)} \pm \frac{(1-x-y)[-b^2(-a\pm a^2\pm\cdots)]}{(1-b^2)} \qquad \text{(D-6)}$$

and

$$a^2 = (\omega_{ce}/\omega)^2,$$

$$b^2 = (\omega_p/\omega)^2,$$

$$c^2 = (\omega_{ce}/\omega)^2 + (\omega_p/\omega)^2.$$

If Eq. (D-5) is substituted into Eq. (3-7) for k_p, the equation for $\Delta\phi$ becomes

$$\Delta\phi = -\int_0^L [(1+z)^{1/2} k_{ord} - k_v] \, dx.$$

Expand $(1+z)^{1/2}$ in the above equation to obtain

$$\Delta\phi = -\int_0^L [(k_{ord} - k_v) + (\frac{z}{2} - \frac{z^2}{8} + \cdots) k_{ord}] \, dx.$$

Substitute the expression for k_{ord}, (Eq. D-1), into the above equation and expand $(1-b^2)^{1/2}$ to obtain

$$\Delta\phi = -(\frac{\omega}{c})^2 \int_0^L [1 - \frac{b^2}{2} - \frac{b^4}{8} - \cdots) - 1 + (\frac{z}{2} - \frac{z^2}{8} + \cdots)$$

$$(1 - \frac{b^2}{2} - \frac{b^4}{8} - \cdots)] \, dx.$$

Neglecting the higher order terms, the equation for $\Delta\phi$ becomes

$$\Delta\phi = \frac{\omega}{2cn_c} \int_0^L n_e(x)(1 - \frac{z}{b^2}) \, dx \qquad \text{(D-7)}$$

which is similar to Eq. (3-8) except for the term $(1-z/b^2)$.

In reference to Fig. 5, the innermost set of magnetic field lines form the plasma boundary. The ellipses are surfaces of constant magnetic induction. Moving from the center outward, these surfaces have values of 260, 540, 820 and 1100 Gauss, 3040 Gauss in the ring cusp region and 5030 Gauss in the point cusp region. In the wave propagation region of interest, the magnetic induction varies from zero to 1000 Gauss. With $B_0 = 1000$ Gauss, $\omega_{ce} = 1.8 \times 10^{10}$ sec^{-1} and $\omega_{ce}/\omega = 0.14$. For an expected electron

density of 1.5×10^{10} cm^{-3}, $\omega_p/\omega = 0.053$. Using these approximations in Eq. (D-6), the error in approximating $\vec{k}_p$ by $\vec{k}_{ord}$ is listed below for possible values of x and y along with the error if the electron density where increased by an order of magnitude.

x	y	error($n_e = 1.5 \times 10^{10}$ cm^{-3})	error(1.5×10^{11} cm^{-3})
0.0	0.0	16.0%	16.5%
0.0	0.8	4.8	5.0
0.0	1.0	2.0	2.1
0.8	0.15	1.1	1.1
1.0	0.0	0.0	0.0

Wave propagation parallel to $\vec{B}_0$ corresponds to x=0 and y=0 while x=1, y=0 corresponds to the ordinary wave. Thus, there is little error in assuming $\vec{k}_p$ to be represented by $\vec{k}_{ord}$.

APPENDIX E

PROPOSED MODIFICATIONS TO THE EXPERIMENTAL DEVICE

The chamber is currently undergoing several modifications. The 3.4 cm ID point cusp ports will be replaced with 5.5 cm ID tubes. The three tubes which connect the chamber to the vacuum system will be removed and the ionization pump will be connected directly to the point cusp port. At the other point cusp, the 5.5 cm tube will be adapted to a 15.2 cm ID "cross" with a small ionization pump attached to the "cross". The effective pumping speed will be increased from 12 liter/sec to approximately 50 liter/sec. Internal heaters will be installed in the chamber for bakeout.

With the larger space in the point cusp, a more rugged electron gun can be constructed using a commercial filament.

Additional coils will be wound and placed over the larger point cusp ports to provide a $B_z \gtrsim 6000$ Gauss.

After sufficient data has been been taken with these improvements, one of the steel rings which was installed and removed earlier will be welded onto the ring anode decreasing the ring anode gap thickness to 0.53 cm. Data will then be taken with the smaller gap thickness to determine the effect of the smaller ring anode dimension on the electron density.